國立交通大學

物理研究所

博 士 論 文

以磁性波電漿尾隨場加速為極高能宇宙射線之

產生機制

Magnetowave Induced Plasma Wakefield Acceleration as
a Production Mechanism for Ultrahigh Energy Cosmic Rays

研 究 生：張鳳吟

指導教授：林貴林　教授

陳丕燊　教授

中 華 民 國 九 十 八 年 七 月

以磁性波電漿尾隨場加速為極高能宇宙射線之產生機制

Magnetowave Induced Plasma Wakefield Acceleration as a
Production Mechanism for Ultrahigh Energy Cosmic Rays

研 究 生：張鳳吟　　　　　　Student：Feng-Yin Chang

指導教授：林貴林　　　　　　Advisor：Guey-Lin Lin

　　　　　陳丕燊　　　　　　　　　　Pisin Chen

國 立 交 通 大 學
物 理 研 究 所
博 士 論 文

A Thesis
Submitted to Institute of Physics
College of Science
National Chiao Tung University
in partial Fulfillment of the Requirements
for the Degree of
Doctor of Philosophy
in

Physics

July 2009

Hsinchu, Taiwan, Republic of China

中華民國九十八年七月

以磁性波電漿尾隨場加速為極高能宇宙射線之產生機制

學生：張鳳吟　　　　　　　　　　　　　　指導教授：林貴林
　　　　　　　　　　　　　　　　　　　　　　　　　陳丕燊

國立交通大學物理研究所

摘　　　要

近幾十年來極高能宇宙射線的來源一直是個未解的謎團。目前一些現有的機制，如震波擴散加速與其他，在解釋這些粒子上仍存在問題。所以根據電漿加速器的概念，我們提出了新的機制—磁性波電漿尾隨場加速—來解釋極高能宇宙射線的產生。這篇論文中，我們以哨波作為電漿尾隨場的驅動脈衝來建立磁性波電漿尾隨場加速的理論及模擬，電漿模擬的結果證實磁性波電漿尾隨場的存在，同時它的場強符合我們新推導的相對論性理論預測；在適當的條件下，我們也證明磁性波電漿尾隨場經過幾百個電漿肌膚深度後仍可以維持高度同調性及高度加速梯度，這樣的特性使磁性波電漿尾隨場可以應用在加速器實驗。在天文環境中，粒子與尾隨場的隨機交互作用讓加速粒子能譜遵守指數律，我們最後說明活躍星系核加速粒子到 10^{21} 電子伏特的可能性。
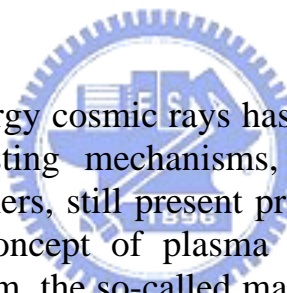
Magneowave Induced Plasma Wakefield Acceleration as a Production Mechanism for Ultrahigh Energy Cosmic Rays

student：Feng-Yin Chang   Advisors：Dr. Guey-Lin Lin
                                                        Dr. Pisin Chen

Institute of Physics
National Chiao Tung University

ABSTRACT

The origin of ultrahigh energy cosmic rays has been puzzled over several decades. So far, the existing mechanisms, such as diffusive shock acceleration (DSA) and others, still present problems in explaining these particles. Based on the concept of plasma wakefield accelerator, we proposed a novel mechanism, the so-called magnetowave induced plasma wakefield acceleration (MPWA) to elucidate the production of ultrahigh energy cosmic rays. In this thesis we establish the general MPWA theory and perform a particle-in-cell simulation that provides the evidence of the generation of magnetowave induced plasma wakefield. Here we invoke the high frequency and high speed whistler mode for the driving pulse. The plasma wakefield obtained in the simulation compares favorably with our newly developed relativistic theory of MPWA. We show that under appropriate conditions, the plasma wakefield maintains very high coherence and sustains high-gradient acceleration over hundreds of plasma skin depths. In astrophysical setting, the power-law spectrum and accelerating gradient are given in the theory. Invoking AGNs as the acceleration site, we will show that the particle accelerated to 10^{21}eV is possible.

Contents

List of Figures

Chapter 1

Introduction

1.1 The Origin of Ultrahigh Energy Cosmic Rays

The origin of ultrahigh energy cosmic rays (UHECR) has been a long-standing mystery in astrophysics. According to the detection of the giant air showers, the arrival of UHECR with energy up to 10^{20} eV was confirmed[1, 2, 3] and the most energetic cosmic particle recorded was about $\sim 3 \times 10^{20}$ eV by the Fly's Eye Observatory[2]. It is amazing that a subatomic particle can carry macroscopic kinetic energy equal to that of a baseball (142 g) traveling at 96 km/h. Having such high energy, UHECRs pose a serious challenge on the theoretical models.

Figure 1.1 shows the overall cosmic ray spectrum which simply follows a power law with index roughly -3. There are two kinks at energy 10^{15} eV(the knee) and 10^{18} (the ankle) eV denoting the changes of the power-law indices. We believe that the ankle is due to the transition of galactic source to extra-galactic sources and the change of composition. In addition, beyond energy 5×10^{19} eV, the flux is expected to drop significantly due to the GZK effect taking place. The GZK effect was proposed in 1967 soon after the discovery of the cosmic microwave background (CMB) by Greisen, Zatsepin, and Kuzmin (GZK)[4, 5]. A cosmic protons with energy above the threshold (the GZK cutoff energy) would lose its energy through interaction with the CMB photons. As a result its spectrum would be subject to a cutoff. In the observation aspect, HiRes which uses the fluorescence method clearly exhibits a GZK suppression
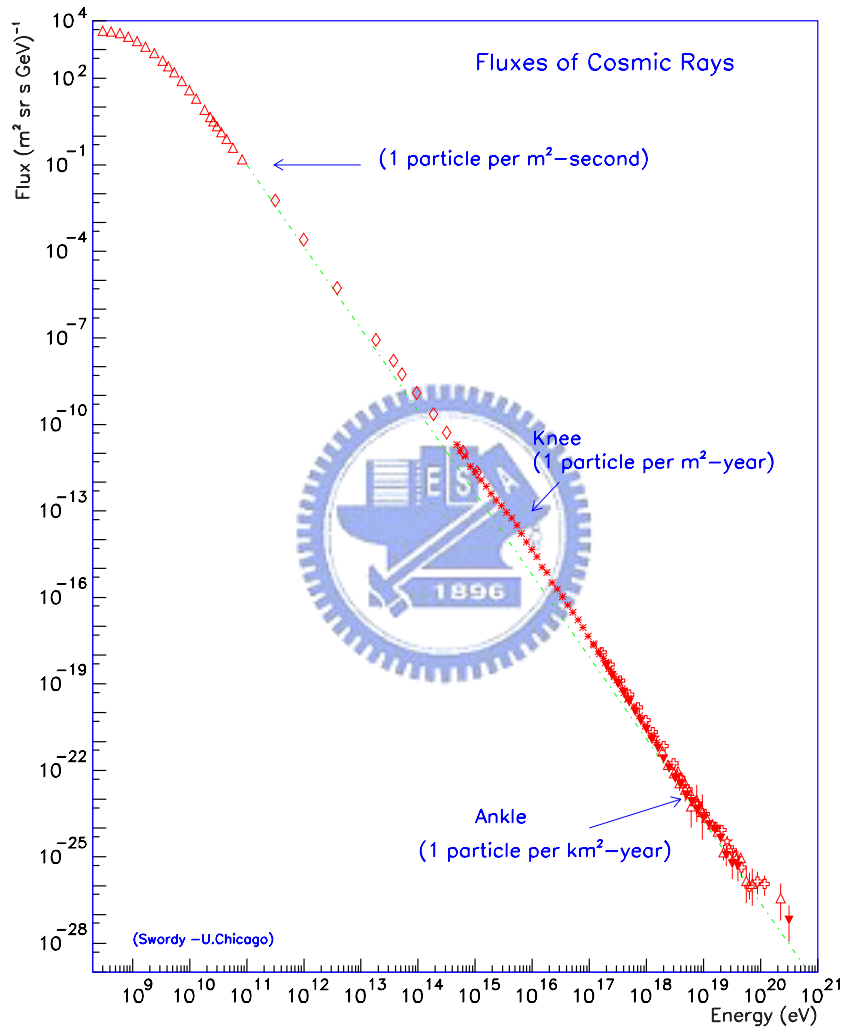
Figure 1.1: The cosmic ray spectrum.

signature, while AGASA instead shows a continue spectrum. This discrepancy deeps the puzzle of UHECR. Fortunately precision measurements[6, 7] on the yield of air-shower induced fluorescence lend support to the energy calibration of the HiRes observations[8]. Together with the recent data from the Pierre Auger Observatory[9] which exhibits a similar location of an "ankle" and the GZK suppression as those observed in HiRes, we confirm the validity of the GZK mechanism. Nevertheless both AGASA and HiRes presented the existing of super-GZK events, which are not observed by Auger. It implies that the super-GZK particles should have original energies even higher and be restrictively located within $50 \sim 75 Mpc$ (the GZK attenuation length). However so far there is no source within this range identified response for the UHECR production.

There has been many mechanisms caming up with to solve the UHECR production issues. Thus far, the existing theories can be broadly categorized into two scenarios, top-down and bottom-up. The bottom-up model relies on an efficient acceleration mechanism for an ordinary particle, such as a proton, at some astrophysical site to ultra high energies. While the top-down scenario is an alterative model to the bottom-up scenario proposed in order to explain the super-GZK events. It resorts to the decay of some relics of Grand Unified scale ($\sim 10^{24}$ eV) from the early universe. The main challenges for the scenarios are their difficulties of complying with the observed event rates and the energy spectrum[10], and the fine-tuning of particle lifetimes. Meanwhile the top-down theories would predict high fluxes of photon and neutrino as the side products. The lack of observation of photons or neutrinos strongly disfavors these models[11, 12]. Therefore finding a viable bottom-up mechanism to accelerate ordinary particles beyond 10^{20} eV becomes more acute.

1.2   Conventional Model

1.2.1   Diffusive Shock Acceleration

The first idea of the cosmic ray acceleration mechanism yielding a power law spectrum is proposed by Fermi in 1949[13]. He considered that cosmic particles in interstellar space can diffuse by scattering off the randomly moving mag-

netic clouds, resulting in an average energy gain per encounter proportional to the mean velocity square of the magnetic clouds. It is often referred to as the second-order Fermi acceleration. Particles can be accelerated to high energy by many turns of the accelerating cycles. However the mechanism is not efficient because the process is non-relativistic and the energy gain proportionally to β^2 is accordingly small. As a variant of Fermi mechanism in strong non-relativistic shocks, the so-called diffusive shock acceleration(DSA) mechanism, was independently proposed by several authors [14, 15, 16, 17] in the late 1970s. It is referred to as the first order Fermi mechanism. This mechanism was conventionally accepted as the origin of the high energy cosmic ray. According to the simple picture from Bell[14], the upstream particles injected crossing the shock front could be turned back by scattering off the magnetic turbulence generated in downstream and vice versa, resulting in the diffusion of particles on the both sides of shock front. Different from the Fermi mechanism, each crossing can gain energy proportional to the first power of shock velocity. It is because the particles at shock always encounter head-on collisions.

These two mechanisms both produce power law spectrums. Assuming the energy gain per encounter is $\Delta\epsilon/\epsilon = \xi$, the energy after n encounters is,

$$\epsilon_n = \epsilon_0(1+\xi)^n \tag{1.1}$$

where ϵ_0 is the energy at injection into the accelerator. If the probability of escape from the acceleration region is P_{esc} per encounter, then the probability of remaining in the acceleration region after n encounters is $(1-P_{esc})^n$. The number of encounters needed to reach energy E is

$$n = \ln\left(\frac{\epsilon}{\epsilon_0}\right)/\ln(1+\xi). \tag{1.2}$$

Thus, the proportion of particles with energy greater than E is

$$N(>\epsilon) \propto \sum_{m=n}^{\infty}(1-P_{esc})^m = \frac{(1-P_{esc})^n}{P_{esc}}. \tag{1.3}$$

Substituting the expression of n into Eq. (1.3), we arrive at the power-law spectrum

$$N(>\epsilon) \propto \frac{1}{P_{esc}}\left(\frac{\epsilon}{\epsilon_0}\right)^{-\gamma}, \tag{1.4}$$

with

$$\gamma = \ln\left(\frac{1}{1-P_{esc}}\right)/\ln(1+\xi) \approx \frac{P_{esc}}{\xi} \tag{1.5}$$

From Fermi's picture, the probability per encounter of escape from the acceleration region P_{esc} is the ratio of the characteristic time for the acceleration cycle and the escape from the acceleration region. This resulting spectral index is not universal, but depends on the properties of the magnetic clouds. For the strong shock case, it can be shown that at a shock,

$$\gamma = \frac{P_{\text{esc}}}{\xi} = \frac{3}{u_u/u_d - 1} \tag{1.6}$$

with

$$\frac{u_u}{u_d} = \frac{(c_p/c_v + 1)M^2}{(c_p/c_v - 1)M^2 + 2} \tag{1.7}$$

given by Rankine-Hugoniot jump conditions at the shock front[18]. Here u_u and u_d are the velocities of gas flows in upstream and downstream respectively and the Mach number M is defined as the ratio of u_u to the sound speed in upstream gas. For an monatomic gas the ratio of specific heats $c_p/c_v = 5/3$, $\gamma \approx 1 + \frac{4}{M^2} \sim 1$ for the strong shock with $M \gg 1$, which is independent of the shock properties and is universal. The differential spectrum provided by diffusive shock acceleration mechanism is given by $dN/dE \propto E^{-2}$ at strong non-relativistic shock.

The above discussions are for non-relativistic shocks. Since the most powerful astrophysics objects often involves ultra relativistic flows, the application of DSA to ultra relativistic flows has also been massively studied over years (see [19]). When considering the relativistic shock, the distribution of scattered particles is no longer isotropic but has orientations on angle. As a consequence, the application of DSA becomes more difficult. The average energy gain $\Delta E' = E'_f - E'_i$ in the rest frame of shock front is shown as order of E'_i itself, hence in the first shock crossing cycle, a large initial boost in energy can be achieved, $E_i/E_f \sim \Gamma^2$ where Γ is the gamma factor of the bulk velocity of relativistic flows[20]. The power-index is fitted about -2.23 ± 0.01 [21, 22].

1.2.2 Limitations

With the successful application to supernova remnants for cosmic ray around the knee (10^{15}) eV, which has been confirmed via the x-ray observation[23], DSA is conventionally considered as the possible solution of high energy cosmic ray.

However DAS relies on the random collisions of the high energy particle against magnetic field domains or the shock media. They restrict the accelerating time from the shock lateral size and the strength of background magnetic field, and therefore the maximum energy gain. At very high energy, the collision process in magnetic turbulence necessarily induces severe synchrotron radiation loss, which is proportional to the fourth power of γ. Compiling above limitations, DAS has difficulties to explain UHECRs. Evidently, novel acceleration mechanisms that can avoid some of the difficulties faced by these conventional models should not be overlooked.

1.3 Plasma Wakefield Acceleration as a Possible Mechanism

Plasma wakefield accelerators[24, 25] are known to possess two salient features: (i) The plasma can support an extremely high "acceleration gradient," i.e., energy gain per unit distance, which does not depend (inversely) on the particlesinstantaneous energy or momentum. This is essential to avoid the gradual decrease of efficiency in reaching ultrahigh energies. (ii) The acceleration field is collinear to the particle momentum. Therefore, bending of the trajectory is not necessary in this mechanism. This helps to minimize inherent energy losses that would be severe at ultrahigh energies.

So motivated by these considerations, it was proposed that UHECR can be produced from the plasma wakefield excited in astrophysical setting[26]. Instead of using laser or charged beam which does not exist in astrophysical environments, Chen et al invoked Alfven shocks as the driving sources to excite plasma wakefields. This idea of using shocks to excite plasma wakefield has attracted several astrophysical plasma physicists [27, 28]. Chen et al showed that the power-law spectrum is accounted for the stochastic encounters between the particles and the randomly generated wakefields. Using the short gamma ray burst(GRB) as the working source, Chen et al obtained the maximum accelerating gradient and predicted the event rate. However, in that paper, their estimation of accelerating gradient was based upon the theory of laser wakefield acceleration without taking the background magnetic effect into account.

Furthermore, this concept has never been validated through computer simulation. Thus, we develop a new mechanism of plasma wakefield (the magnetowave induced plasma wakefield acceleration (MPWA) invoking the high frequency and high speed whistler mode as driving pulse, and confirm this concept via computer simulations[29]. The magnetowave with phase velocity $v_{ph} < c$ has component $|B| > |E|$ in nature. On the other hand the laser and charged beam have $|E| > |B|$.

In this thesis, we will discuss the complete theory of MPWA and its application to UHECR. The content is the following: in Chap.2, the basic plasma physics is viewed to give the way for subsequent discussions. The last section of Chap. 2 introduces the different types of the plasma wakeifled accelerator. In Chap. 3, we start looking at the plasma wakefield acceleration in magnetized plasma. With $\omega \gg \omega_c$, the magnetic field effect can be ignored. In Chap.4, we focus on the driving pulse with $\omega < \omega_c$ (MPWA) and introduce a MPWA condition. The theory of MPWA in linear and nonlinear regimes under the MPWA condition are presented and the limitation of MPWA is also discussed. In Chap. 5, the particle in cell(PIC) code to produce MPWA is introduced. We show that the simulation results are in good agreements with the theoretical prediction. Finally with the theoretical model established, we apply this mechanism to explain the UHECR acceleration. In Chap. 6 we obtain the power-law spectrum from the stochastic process of the wakefield acceleration and estimate the accelerating gradient provided by AGN jets. The summary and conclusion are presented in Chap. 7.

Chapter 2

Basic Concept of Plasma

It is known that 99 percent of visible matter in the universe is in plasma state. All the astrophysical objects, such as stars, relativistic jets, accretion disks, etc.., are made of plasma. Therefore a though understanding of plasma physics could lead to an understanding of 99 percent of the visible universe. Based on that, the idea of plasma wakefield acceleration for UHECR is therefore possible. In this chapter I will briefly introduce the basic concept of plasma. The cgs unit system is used in the following treatment.

2.1   What is Plasma

Plasma is a partially ionized gas consisting of free negative electrons, positive ions and neutral atoms. When we heat a liquid, we can see more and more vapors created as the temperature rises till reaching the boiled point. After that, all liquid molecules are turned into gas molecules. If we continue to heat the gas, some atoms or molecules will eventually get ionized. Thus in addition to the three thermodynamic states, plasma is sometimes referred to as the fourth state of matter. Because the ionized energy of atoms is of the order 10 eV, plasma is usually created in a very high temperature. But in fact, the atoms still have chances to be ionized at the room temperature due to the tail of thermal distribution. The amount of ionization is very rare so that we can not feel the plasma around us. To estimate the portion of ionization in thermal equilibrium, we can use Saha equation[30]

$$\frac{n_i}{n_n} \approx 2.4 \times 10^{15} \frac{T^{3/2}}{n_i} e^{-U_i/kT}, \tag{2.1}$$

where n_i and n_n are the densities of ionized atoms and of neutral atoms respectively, T is the gas temperature in unit of K, and U_i is the ionization energy of the gas. If we take the room temperature T=300K, gas density $n_n \approx 3 \times 10^{19} \text{cm}^{-3}$, and $U_i \approx 14.5$ eV for nitrogen, we can predict the fraction of ionization

$$\frac{n_i}{n_n + n_i} \approx \frac{n_i}{n_n} \approx 10^{-122}$$

which is extremely low.

2.2 Definition of Plasma

Not any ionized gas can be called a plasma. As mentioned above, there is always some small fraction of ionization in any gas. So the plasma is defined from its most important properties, collectiveness and the quasi-neutrality. Since plasma contains charged particles, the moves of these charges can generate local concentrations of positive or negative charges which give rise to electric fields. The motions of charges also generate currents and then the magnetic fields. These fields are long-range and could affect the motions of other charged particles far away. To see the effect, let us imagine two small charged regions of plasma separated by a distance r. Even if the Coulomb interaction between the two individual charged particles diminishes as $1/r^2$, for a given solid angle, one region can feel a total force from the other region with volume increasing as r^3. Therefore, elements of plasma can experience a force on one another even at large distances. By "collectiveness" we mean that plasma motions depend not only on local conditions but on the state of the plasma in remote regions as well.

The quasi-neutrality comes from a fundamental characteristic of the plasma, which is the capability to shield out electric potentials that are applied to it. Suppose we set up an electric field by inserting a ball charged with positive charges, the ball would naturally attract an electron cloud with the same amount of positive charges surrounded. If we assume an electron distribution

which follows the Boltzman's equation so that

$$n_e(\Phi) = n_0 e^{e\Phi/k_B T} \tag{2.2}$$

where Φ, is the potential associated with the slight separation of electrons and ions, n_0 is the plasma density at $\Phi = 0$ and T is the electron temperature. Since an ion is 1800 times heavier than an electron, the ion background can be regarded as motionless. Therefore the ion density n_i, where the subscript i denotes the ion background, is approximately equal to the plasma density n_0. Considering only the one-dimensional case, the Poisson equation turns into with Eq. (2.2)

$$\frac{\partial^2 \Phi}{\partial z^2} = 4\pi e n_0 \left(e^{e\Phi/k_B T} - 1 \right). \tag{2.3}$$

In the region where $|e\Phi/k_B T| \ll 1$, we can expand the exponential to the first order,

$$\frac{\partial^2 \Phi}{\partial z^2} = 4\pi e n_0 \left(\frac{e\Phi}{k_B T} + \cdots \right) \tag{2.4}$$

that gives the solution of Φ

$$\Phi = \Phi_0 e^{-|z|/\lambda_D} \tag{2.5}$$

with the characteristic length λ_D defined as

$$\lambda_D = \sqrt{\frac{kT}{4\pi n e^2}} = v_{th}/\omega_p \tag{2.6}$$

where $\omega_p \equiv \sqrt{4\pi e^2 n_0/m}$ is the plasma neutral frequency and $v_{th} = \sqrt{k_B T/m}$ is the velocity of electron thermal motion. λ_D is called Debye length, named after the Dutch physicist Peter Debye. If the plasma is cold, $T = 0$, then $\lambda_D = 0$ and the shielding is perfect. It allows no electric field being presented outside the electron cloud. However if $T \neq 0$, λ_D is accordingly finite. The potential will be no longer perfectly shielded but decay exponentially with the distance. Because of the shielding, the distant particles will not feel the existence of the charged ball in the plasma. Therefore for remaining the quasi-neutrality, the condition for a plasma is $\lambda_D \gg L$, where L is the plasma size. In addition, the Debye shielding itself is actually a statistic concept. Thus for the validity of Debye shielding, we should compute the number of particles in a Debye sphere g and require

$$g \equiv n\frac{4}{3}\pi\lambda_D^3 = 1380T^{3/2}n^{1/2} \ggg 1, \tag{2.7}$$

where $n = n_e = n_i$ is the plasma density and g is called the plasma parameter. Combining the two conditions, we can make the criteria for plasma

1) $\lambda \gg L$.

2) $g \ggg 1$.

3) $\omega\tau > 1$.

where ω is the frequency of typical plasma collision and τ is the mean time between collisions. Finally the item 3 requests a low collision rate for plasma.

2.3 Dynamics of Plasma

2.3.1 Fluid Description

Since a typical plasma density might be a huge number of ion-electron pairs per cm^{-3}, it is impossible to deal with each plasma particle. Fortunately, the majority of plasma presents a macroscopic behavior. So we are able to treat plasma as fluids, composed of electrons , ions and neutral atoms. As a result, the motion of individual particle is neglected and only the averaging motion is taken into account. The plasma fluid containing an additional electromagnetic effect is different from an ordinary fluid. Such effect leads to the complexity of plasma, and the varieties of phenomena could occur in a plasma.

In plasma, Maxwell's equations can tell us how $\mathbf{E}$ and $\mathbf{B}$ are associated with a given state of the plasma. To maintain the self-consistency, we include equations that describe the plasma response to the $\mathbf{E}$ and $\mathbf{B}$ field such that

$$
\begin{aligned}
\nabla \cdot \mathbf{E} &= 4\pi e(n_i - n_e) = 4\pi\rho \\
\nabla \times \mathbf{E} &= -\frac{\partial \mathbf{B}}{\partial t} \\
\nabla \cdot \mathbf{B} &= 0 \\
c\nabla \times \mathbf{B} &= 4\pi e(n_i\mathbf{u}_i - n_e\mathbf{u}_e) + \frac{\partial \mathbf{E}}{\partial t} = 4\pi\mathbf{J} + \frac{\partial \mathbf{E}}{\partial t}
\end{aligned}
$$

where ρ and $\mathbf{J}$ are the charge density and charge current given by the plasma, and $\mathbf{u}$ is the fluid velocity of from averaging the total velocity in the fluid unit.

These $\mathbf{E}$ and $\mathbf{B}$ fields above also act back on the plasma species, therefore the equation of motion regarding the electromagnetic force is described,

$$m_j n_j \left[\frac{\partial \mathbf{u}_j}{\partial t} + (\mathbf{u}_j \cdot \nabla)\mathbf{u}_j \right] = q_j(\mathbf{E} + \frac{\mathbf{u}_j}{c} \times \mathbf{B}) - \nabla p$$

where $j = i, e$ stands for fluid of ions and electrons respectively. The m_j is the mass of the fluid element. The equation above is in Eulerian representation, dealing with the time and space derivatives separately. Sometimes we describe the fluid in either Eulerian (the coordinate scheme) or Lagragian(the co-moving scheme) representations. The relation between the two representations is

$$\frac{d}{dt}_{\text{Lagragin}} = \left(\frac{\partial}{\partial t} + \mathbf{v} \cdot \nabla \right)_{\text{Eulerian}}.$$

The second term on the right hand side is called the convective term. Finally combining the above equations and the continuity equation, we obtain the complete set of fluid equations

$$\nabla \cdot \mathbf{E} = 4\pi \sum_j q_j n_j, \tag{2.8a}$$

$$\nabla \times \mathbf{E} = -\frac{\partial \mathbf{B}}{\partial t}, \tag{2.8b}$$

$$\nabla \cdot \mathbf{B} = 0, \tag{2.8c}$$

$$c\nabla \times \mathbf{B} = 4\pi \sum_j q_j n_j \mathbf{u}_j + \frac{\partial \mathbf{E}}{\partial t}, \tag{2.8d}$$

$$\frac{\partial n_j}{\partial t} + \nabla \cdot (n_j \mathbf{u}_j) = 0, \tag{2.8e}$$

$$m_j \left[\frac{\partial \mathbf{u}_j}{\partial t} + (\mathbf{u}_j \cdot \nabla)\mathbf{u}_j \right] = q_j(\mathbf{E} + \frac{\mathbf{u}_j}{c} \times \mathbf{B}) - \frac{\nabla p_j}{n_j}, \tag{2.8f}$$

$$p_j = C(m_j n_j)^{\gamma_j}. \tag{2.8g}$$

with 11 unknowns $(\mathbf{E}, \mathbf{B}, \mathbf{u}, n, p)$ for each species. Here Eq. (2.8e) is the continuity equation and the last equation is the equation of state, with C a constant and $\gamma = C_p/C_v$ the ratio of specific heats.

2.3.2 Kinetic Description

Beside the fluid theory, the alternative way to describe plasma is the kinetic theory. In most cases, the fluid equations can solve the plasma problems with acceptable good accuracy. But for some special cases, such as the instabilities, the fluid treatment will be inadequate. Thus, we directly look at the distribution

function $f_j(\mathbf{r}, \mathbf{v}, t)$ for each plasma species (here $\mathbf{v}$ is the individual velocity). By knowing the distribution function, we are able to derive the macroscopic physical variables from integrating the function over all velocity spaces. This treatment is called kinetic theory.

The time evolution of distribution function $f_j(\mathbf{r}, \mathbf{v}, t)$ is govern by the Boltzmann equation,

$$\frac{df_j}{dt} = \frac{\partial f_j}{\partial t} + \mathbf{v}_j \cdot \nabla f_j + \frac{q_j}{m_j}(\mathbf{E} + \frac{\mathbf{v}_j}{c} \times \mathbf{B}) \cdot \nabla_\mathbf{v} f_j = (\frac{\delta f_j}{\delta t})_c, \qquad (2.9)$$

where $(\delta f_j/\delta t)_c$ is the collision term. The plasma density can be obtained from

$$n_j(\mathbf{r}, t) = \int_\mathbf{v} f_j(\mathbf{r}, \mathbf{v}, t) d^3 v,$$

and the average velocity $\mathbf{u}_j$ is given by

$$\mathbf{u}_j(\mathbf{r}, t) = \frac{\int_\mathbf{v} \mathbf{v} f_j(\mathbf{r}, \mathbf{v}, t) d^3 v,}{\int_\mathbf{v} f_j(\mathbf{r}, \mathbf{v}, t) d^3 v}$$

If the plasma is collisionless, the collision term vanishes and Eq. (2.9) takes the form

$$\frac{\partial f}{\partial t} + \mathbf{v} \cdot \nabla f + \frac{q}{m}(\mathbf{E} + \frac{\mathbf{v}}{c} \times \mathbf{B}) \cdot \nabla_\mathbf{v} f = 0, \qquad (2.10)$$

where we drop the subscript j. This is called the Vlasov equation, most commonly studied in the kinetic theory. Regardless of the collision term, the zero moment of Eq. (2.9) is obtained by integrating over the velocity space,

$$\int \frac{\partial f}{\partial t} d\mathbf{v} + \int \mathbf{v} \cdot \nabla f d\mathbf{v} + \frac{q}{m} \int (\mathbf{E} + \frac{\mathbf{v}}{c} \times \mathbf{B}) \cdot \nabla_\mathbf{v} f d\mathbf{v} = 0 \qquad (2.11)$$

and the next moment is obtained by multiplying $m\mathbf{v}$ to the equation and integrating over $\mathbf{v}$ such that

$$m \int \mathbf{v} \frac{\partial f}{\partial t} d\mathbf{v} + m \int \mathbf{v}(\mathbf{v} \cdot \nabla) f d\mathbf{v} + q \int \mathbf{v}(\mathbf{E} + \frac{\mathbf{v}}{c} \times \mathbf{B}) \cdot \nabla_\mathbf{v} f d\mathbf{v}$$
$$= 0. \qquad (2.12)$$

Taking the above two moments of the Boltzmann's equation leads to the continuity equation Eq. (2.8e) and the equation of motion of fluid(2.8f). We show that the fluid theory can be derived from the kinetic theory; therefore the fluid and kinetic representations of plasma are equivalent.

2.4   Waves in the Plasma

We have already established the complete set of fluid equations for plasma. To solve these equations, we introduce the perturbation theory describing a small deviation of physical quantities to their equilibrium state. These quantities can be decomposed into the equilibrium solution plus a small perturbation. After taking the Fourier expansion, the perturbations are transformed into a superposition of sinusoidal oscillations in different frequencies. As a result the fluid equations Eq. (2.8a) to (2.8g) can be linearized in (ω, k) space and the resulting equations are easier to solve. In this section, I review the physics of plasma oscillation and electromagnetic wave in plasma for demonstrating the technique for solving the fluid equations.

2.4.1   Plasma Oscillation

When the electrons in plasma are displaced by some perturbations from a uniform background of ions, electric fields are built up in such a direction as to restore the neutrality of the plasma by pulling the electrons back to their original positions. Because of their inertia, the electrons will overshoot and oscillate around their equilibrium positions. The process is known as the plasma oscillation, also known as Langmuir wave, with a characteristic frequency ω_p[31]. To derive the expression for the plasma frequency ω_p, we solve the fluid equation in the simplest case that (1) $B = 0$, there is no magnetic field; (2) $T = 0$, hence $\nabla p = 0$, there are no thermal motions; (3) background ions are fixed; (4) the electron motions only take place along to z direction. The fluid equations in this simplification are obtained,

$$mn_e \left[\frac{\partial \mathbf{v}_e}{\partial t} + (\mathbf{v}_e \cdot \nabla)\mathbf{v}_e \right] = -en_e\mathbf{E} \tag{2.13a}$$

$$\frac{\partial n}{\partial t} + \nabla \cdot (n_e\mathbf{v}_e) = 0 \tag{2.13b}$$

$$\nabla \cdot \mathbf{E} = 4\pi e(n_i - n_e), \tag{2.13c}$$

with electron fluid velocity $\mathbf{u}_e$ replaced by $\mathbf{v}_e$ for convenience. Since the plasma is assumed to be slightly perturbed, the variables in the equations can be separated into two parts: the equilibrium part, subscripted by 0, and the perturba-

tion part by 1 that

$$n_e = n_0 + n_1,$$

$$\mathbf{v}_e = \mathbf{v}_0 + \mathbf{v}_1,$$

$$\mathbf{E} = \mathbf{E}_0 + \mathbf{E}_1.$$

If the plasma is initially stationary, we have the equilibrium state $\nabla n_0 = \mathbf{v}_0 = \mathbf{E}_0 = 0$. The fluid equations are then given by

$$m\frac{\partial \mathbf{v}_1}{\partial t} = -e\mathbf{E}_1, \tag{2.14a}$$

$$\frac{\partial n_1}{\partial t} + n_0 \nabla \cdot \mathbf{v}_1 = 0, \tag{2.14b}$$

$$\nabla \cdot \mathbf{E}_1 = -4\pi e n_1, \tag{2.14c}$$

where the convective term

$$(\mathbf{v} \cdot \nabla)\mathbf{v} = (\mathbf{v}_1 \cdot \nabla)\mathbf{v}_1$$

vanishes due to the higher order perturbation. For plasma oscillation, it is assumed that the quantities oscillate sinusoidally and,

$$n_1 = n_1 e^{i(kz - \omega t)}$$

$$\mathbf{v}_1 = v_1 e^{i(kz - \omega t)}\hat{\mathbf{z}}$$

$$\mathbf{E}_1 = E_1 e^{i(kz - \omega t)}\hat{\mathbf{z}}.$$

So the time derivative $\partial/\partial t$ can be replaced by $-i\omega$ and the space derivative ∇ can be replaced by $i\mathbf{k}$ in the equations. Then the differential equations Eq. (2.14a) to (2.14c) are linearized such that,

$$-im\omega v_1 = -eE_1 \tag{2.15a}$$

$$-i\omega n_1 + n_0 ik v_1 = 0 \tag{2.15b}$$

$$ik \cdot E_1 = -4\pi e n_1. \tag{2.15c}$$

where E_1, which is associated with the plasma oscillation, is an electrostatic field along the k direction. We can rewrite Eq. (2.15a) by applying Eq. (2.15b) and (2.15c) as

$$\left(\omega^2 - \frac{4\pi n_0 e^2}{m}\right)v_1 = 0. \tag{2.16}$$

Eq. (2.16) is the dispersion relation for the plasma oscillation. Because there is no k dependence in this expression, the plasma oscillation does not depend on the wavelength. Hence the phase velocity defined as ω/k and the group velocity defined as $\partial\omega/\partial k$ are both zero. When v_1 is finite, a non trivial solution for Eq. (2.16) requires terms in the parentheses to be 0. Therefore the frequency

$$\omega = \omega_p \equiv \left(\frac{4\pi n_0 e^2}{m}\right)^{1/2}. \tag{2.17}$$

is defined as the plasma frequency. Numerically, with the known physical parameter numbers, one can make the approximate formula

$$f_p \approx 9000\sqrt{n_0}$$

which only depends on the plasma density. So far the treatments are all done in cold plasma case ($T = 0$). For warn plasma ($T \neq 0$), the pressure term ∇p should be taken into account in Eq. (2.13a). The dispersion relation then becomes

$$\omega^2 = \omega_p^2 + \left(\frac{\gamma_B k_B T}{m}\right) k^2, \tag{2.18}$$

where $(\gamma_B k_B T/m)^{1/2}$ is the electron sound speed and the γ_B, usually taken to be 1 in the isothermal sate, is the adiabatic constant for the pressure term Eq. (2.8g). So that the plasma oscillation starts to propagate asymptotically with electron sound speed. Such wave is called the electron acoustic wave.

2.4.2 Electromagnetic Wave in Plasma

Next we study the case of electromagnetic waves in plasma. When an electromagnetic wave travels through a plasma, its associated electromagnetic field shall push the charged particles from their original states and the resulting plasma motions will induce the currents that contribute back to the fields themselves. As a consequence, the dispersion relation of the electromagnetic wave in the plasma contains the plasma effect. If there is no magnetic background field, $B_0 = E_0 = 0$, the electric and magnetic fields in plasma, denoted by $\mathbf{E}_1$ and $\mathbf{B}_1$, are related to each other according to the Maxwell equations

$$\nabla \times \mathbf{E}_1 = -\frac{1}{c}\frac{\partial \mathbf{B}_1}{\partial t} \tag{2.19}$$

$$\nabla \times \mathbf{B}_1 = \frac{4\pi}{c}\mathbf{J}_1 + \frac{1}{c}\frac{\partial \mathbf{E}_1}{\partial t} \tag{2.20}$$

where the term $(4\pi/c)\mathbf{J}_1 \equiv -(4\pi/c)en_0\mathbf{v}_1$ is the plasma current. Taking the time derivative on Eq. (2.20), we combine the above two equations and obtain

$$c^2\nabla \times (\nabla \times \mathbf{E}_1) = 4\pi en_0\frac{\partial \mathbf{v}_1}{\partial t} + \frac{\partial \mathbf{E}_1}{\partial t}. \qquad (2.21)$$

Here $\mathbf{v}_1$ is directly related to the oscillating electric field because the second force term $\mathbf{v}_1/c \times \mathbf{B}_1$ in Eq. (2.8f) is neglected since it is of the second order. Assuming a plane wave varying as $\exp[i(kz - \omega t)]$, the electron velocity $\mathbf{v}_1$ is given by

$$-i\omega\mathbf{v}_1 = -\frac{e}{m}\mathbf{E}_1. \qquad (2.22)$$

We then rewrite Eq. (2.21) as

$$-c^2\mathbf{k} \times (\mathbf{k} \times \mathbf{E}_1) = -i4\pi en_0\omega\mathbf{v}_1 - i\omega\mathbf{E}_1. \qquad (2.23)$$

Substituting Eq. (2.22) to Eq. (2.23), we obtain

$$-\mathbf{k}(\mathbf{k} \cdot \mathbf{E}_1) + k^2\mathbf{E}_1 = -\frac{4\pi e^2 n_0}{mc^2}\mathbf{E}_1 + \frac{\omega^2}{c^2}\mathbf{E}_1. \qquad (2.24)$$

We note that $\mathbf{k} \cdot \mathbf{E}_1 = 0$ because the wave is transverse. Then the equation can be rearranged as

$$\left(k^2 + \frac{\omega_p^2}{c^2} - \frac{\omega^2}{c^2}\right)\mathbf{E}_1 = 0. \qquad (2.25)$$

, which leads to the dispersion relation for electromagnetic wave in unmagnetized plasma.

$$\omega^2 = \omega_p^2 + k^2c^2. \qquad (2.26)$$

We can calculate the phase velocity v_{ph} by using this dispersion relation and obtain

$$v_{ph} = \frac{\omega}{k} = \frac{c}{\sqrt{1 - \frac{\omega_p}{\omega}}} > c. \qquad (2.27)$$

The phase velocity is real only when $\omega > \omega_p$. Therefore a threshold of frequency exists for the electromagnetic wave to penetrate into the plasma. If the wave has frequency $\omega < \omega_p$, it will be reflected by the plasma surface and decays exponentially in the plasma within a skin depth defined as c/ω_p. This concept

is the working principle for radio station to transmit the signals. Similarly, The group velocity can be calculated as

$$v_g = \frac{\partial \omega}{\partial k} = \frac{c^2}{v_{ph}}.$$ (2.28)

Clearly v_g is always smaller that the speed of light c.

2.5   Plasma Wakefield Acceleration

It has been 30 years since T. Tajima and J. Dawson proposed plasma as an accelerator[24], to transfer electromagnetic energy from a laser pulse into the kinetic energy of the accelerated electron by letting the short laser pulse excites large-amplitude plasma waves. In fact the "plasma wave" we call here is the plasma oscillation but having a phase velocity exactly equal to the pulse speed. An electrostatic field relate to this plasma wave is called plasma wakefield. If its phase velocity is closed to the speed of light, a test particle with similar velocity injected to its accelerating phase can surf on the wave and continually gain energy from it. The characteristic accelerating gradient for the plasma wakefield is $G = eE_{wb} = mc\omega_p \sim \sqrt{n_0[\text{cm}]^{-3}}$ Since the mechanism provides a great accelerating gradient which can accelerate charged particles to very high energy in a short distance, it is very attractive to accelerator physics, plasma physics and astrophysics.

Since then there has been several reviews discussing about the plasma based accelerators [32, 33, 34]. So far there have been three plasma wakefield accelerators utilizing laser pulses: laser wakefield accelerator(LWFA), plasma beat-wave accelerator(PBWA) and self-modulated LWFA (SM-LWFA)[32]. In the PBWA [24, 35], two long pulse laser beams with frequencies differed by ω_p are used to resonantly excite the plasma wave. This method was first proposed as an alternative to the laser wakefield accelerator because of the lack of technology for generating ultra-intense picosecond laser pulses at that time. The last one SM-LWFA is somewhat similar to LWFA with a single short pulse but operated at higher density[36, 37, 38]. Therefore SM-LWFA involves a longer length that $L > \lambda_p$ and slightly larger laser power P than the critical power $P_c = 17\omega_2/\omega_p^2$ for relativistic optical guiding. In the high density regime, the pulse becomes self-modulated at the plasma period due to the self-modulation

instability [39, 40, 41]. Then the plasma wave is generated coinciding with the modulated regime. Instead of utilizing laser as driving pulses, Chen et al in 1985 proposed another way to excite the plasma wake by using the charged particle beams [25]. The charged particle which moves relativistically generates the quasi-perpendicular electric field in the lab frame and the magnetic field as well according to the relativistic dynamics. Therefore the charged particle beams behave similar to the laser pulse and the dynamics of plasma wakefield for the two schemes was also shown to be similar by Ruth and Chen[42].

However, either laser beam or charged particle beam is the external impulse and could not be found in the astrophysical environment. Motivated by the ultrahigh energy cosmic ray acceleration issue, Chen, Tajima and Takahashi in 2002 proposed the third type of plasma wakefield acceleration invoking Alfven-shocks as the driving pulses. Different from the laser and the particle beam, Alfven wave is a medium wave which only exist with the support from plasma. Therefore the wakefield driven by Alfven wave is more relevant to the astro-physical settings. F. Y. Chang et al. [29] extended the concept to the high frequency mode (whistler wave). According to Maxwell's equations, these waves have the B component exceeding the E component since their phase velocities are less than the speed of light. We categorize such wave as "magnetowave". In the following chapters, I will discuss the plasma wakefield in magnetized plasma and introduce the theory of magnetowave induced plasma wakefield ac-celeration (MPWA) in both linear and nonlinear regimes. I will also present a self-consistent plasma simulation which is performed to validate this theory.

Chapter 3

Plasma Wakefield in Magnetized Plamsa I

We have studied the dispersion relation of electromagnetic wave traveling in plasma (Eq. (2.26)). Once the plasma is imposed a background magnetic field, the electromagnetic wave presents various different modes at arbitrary angles to the external magnetic field. Among that, we concentrate on the modes parallel to the external magnetic field for our purpose to ensure the linear acceleration that minimizes the energy loss. With the parallel background magnetic field B_0, the electromagnetic wave becomes circularly polarized and its dispersion relation is given by

$$\omega^2 = k^2 c^2 + \frac{\omega_{ip}^2}{1 \pm \omega_{ic}/\omega} + \frac{\omega_p^2}{1 \mp \omega_c/\omega} \, , \tag{3.1}$$

where the upper (lower) signs denote the right-hand (left-hand) circularly polarized waves. $\omega_c = eB_0/mc$ is the electron cyclotron frequency and the subscript i denotes the ion species. Each polarization has two real solutions with high and low frequency branches and both have a frequency cutoff which forms a forbidden gap for wave propagation. Figure 3.1 exhibits the solution of all possible modes and the light curve in vacuum (dashed line) is superimposed. Above the light curve, there are two curves labeled L and R waves to stand for the left-handed and right-handed circularly polarized electromagnetic waves respectively. Whereas the two solutions below the light curve are the whistler
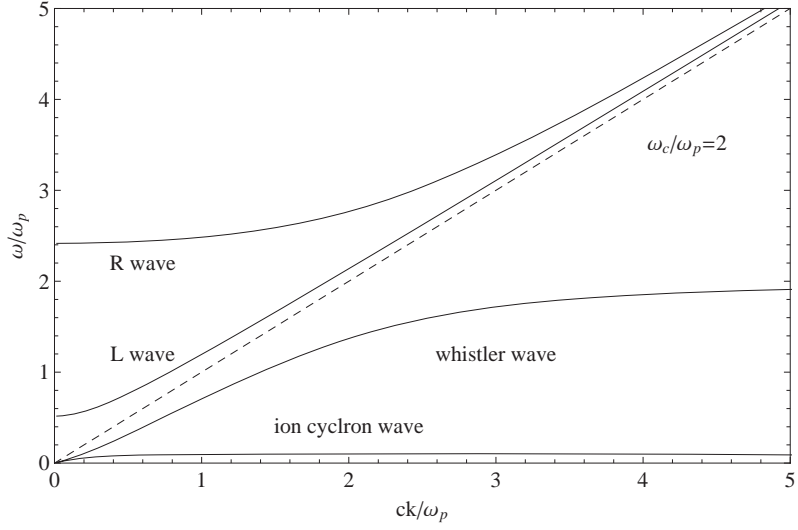
Figure 3.1: The full solutions of Eq. (3.1) with $\omega_c/\omega_p = 2$. The two curves (R and L waves) above the light curve (dashed line) would have $v_{ph} > c$ and the two curves (whistler wave and ion cyclotron wave) below the light curve would have $v_{ph} < c$.

wave and the ion cyclotron wave, having a lower phase velocity than the speed of light. We call such waves the "magnetowaves" because of their exceeding B components in all reference frames. To explain the production of UHECR, Chen et al proposed Alfven shocks as the driving pulses for plasma wakefield. Since the Alfven wave is an ion wave, having very low frequency and low phase velocity, it was the first idea of magnetowave induced plasma wakefield acceleration (MPWA).

In fact the non-relativistic plasma wakefield in magnetized plasma was first studied by P. K. Shukla[43] in 1994. Shukla introduced the ponderomotive force from a circularly polarized electromagnetic pulse that is applicable for all frequency range to excite the plasma wakefield. However he only addressed the upper branch issue (the laser case) in his calculation. For R and L waves which have frequencies $\omega \gg \omega_c$, the dispersion relation Eq. (3.1) can be reduced to that in unmagnetized plasma. Therefore the background magnetic field doesn't play a significant role to the wakefield excitation. Whereas the wakefield induced by the wave with $\omega < \omega_c$ will greatly determined by the ratio of ω_c/ω. In the

following two chapters we will discuss the physics of wakefield induced in the two branches $\omega \gg \omega_c$ (the laser limit) and $\omega < \omega_c$ (magnetowaves). The general theory of MPWA is established in the next chapter.

3.1   General Formulation

In the laser plasma interaction community, the related fields in one dimension along the z direction are often described by the normalized scalar potential $\phi(z,t) \equiv e\Phi(z,t)/mc^2$ for the plasma electrostatic field (plasma wakefield) and the normalized vector potential $\mathbf{a}(z,t) \equiv e\mathbf{A}(z,t)/mc^2$ for the laser field. We have $A_z = 0$ if choosing the Coulomb gauge $\nabla \cdot \mathbf{A} = 0$. The peak of the normalized vector potential a_0, called laser strength parameter by the plasma community, is often used to determine the strength of the driving laser. Since the vector potential $\mathbf{A}$ is the spacial component of the 4-vector $(\rho, \mathbf{A})$, the transverse components of $\mathbf{A}_\perp$ (A_x, A_y) are Lorentz invariant in any reference frame boosting along z direction. As a result, the a_0 by definition is also a Lorentz invariant quantity. In MPWA study, we still follow the convention for laser case. The plasma field $\phi(z,t)$ is governed by the set of fluid equations

$$\frac{\partial^2 \phi}{\partial z^2} = k_p^2 \left(\frac{n}{n_0} - 1 \right), \tag{3.2a}$$

$$\frac{\partial n}{\partial t} + c\frac{\partial}{\partial z}(n\beta_z) = 0, \tag{3.2b}$$

$$\frac{d}{dt}(\gamma\boldsymbol{\beta}_\perp) = \frac{d\mathbf{a}}{dt} - i\omega_c\boldsymbol{\beta}_\perp, \tag{3.2c}$$

$$\frac{d}{dt}(\gamma\beta_z) = c\frac{\partial \phi}{\partial z} - \frac{e}{mc}(\beta_x B_y - \beta_y B_x), \tag{3.2d}$$

$$\frac{d\gamma}{dt} = -\frac{e}{mc}(\beta_x E_x + \beta_y E_y + \beta_z E_z), \tag{3.2e}$$

with ignoring the ion motions. The influence of background magnetic field only takes place in the transverse momentum equation (Eq. (3.2c)), see Appendix A. In these equations, we may neglect the thermal effect due to the assumptions: (i) the electron quiver motion is much greater than the electron thermal motion (ii) the plasma temperature is so low that the thermal energy spread is not sufficient for the plasma to be trapped by the plasma wave. The Lorentz γ of plasma here defines $(1 - \beta_\perp^2 - \beta_z^2)^{-1/2}$ and the ω_c in Eq. (3.2c) gives the influence from the external magnetic field. While the normalized vector potential $\mathbf{a}(z,t)$

22

satisfies the wave equation

$$\left[\frac{\partial^2}{\partial z^2} - \frac{1}{c^2}\frac{\partial^2}{\partial t^2}\right]\mathbf{a} = k_p^2 \frac{n}{n_0}\boldsymbol{\beta}_\perp. \tag{3.3}$$

$k_p \equiv \omega_p/c$ is the plasma wavenumber.

3.2 Laser Wakefield Acceleration

Since the technology of high field laser has been well developed in a laboratory, laser wakefield acceleration is widely studied because of the possibility to the next generation of high accelerating gradient accelerators. When the driving pulse with frequency $\omega \gg \omega_c$ (or $\omega_c \to 0$), the dispersion relation of the pulse approximates to that in unmagnetized plasma case. It is reasonable to study the LWFA mechanism under this limitation. Based on this consideration, the right hand side of Eq. (3.2c) can be ignored and Eq. (3.2c) is rewritten as

$$\frac{d}{dt}(\gamma\boldsymbol{\beta}_\perp - \mathbf{a}) = 0. \tag{3.4}$$

Therefore the transverse canonical momentum $\gamma\boldsymbol{\beta}_\perp - \mathbf{a}$ is conserved and the transverse velocity $\boldsymbol{\beta}_\perp = \mathbf{a}/\gamma$ is easily obtained. Substituting the transverse velocity expression into Eq. (3.2d), we rewrite the Lorentz force in terms of the normalized vector potential $\mathbf{a}$

$$\frac{d\gamma\beta_z}{dt} = c\frac{\partial\phi}{\partial z} - c\frac{1}{2\gamma}\frac{\partial a^2}{\partial z} \tag{3.5}$$

where the second term on the right hand side is the ponderomotive force, the average of the second order Lorentz force. It is on the opposite direction to the gradient of laser intensity and is independent of the charge sign. Thus the electrons within the pulse are pushed away from the center and leave a positive region (ions are only barely moved by the same force), which generates the plasma wakefield.

3.2.1 Linear Regime

With the full set of fluid equations, we first study LWFA in the non-relativistic regime where $\gamma \sim 1$. In this regime, $\beta_\perp$ is equal to $a \ll 1$ so that the condition

for non-relativistic is $a \ll 1$. Hence the complete set of fluid equations can be rewritten as

$$\frac{\partial^2 \phi}{\partial z^2} = k_p^2 N, \tag{3.6a}$$

$$\frac{\partial N}{\partial t} + c\frac{\partial}{\partial z}(\beta_z) = 0, \tag{3.6b}$$

$$\frac{\partial \beta_z}{\partial t} = c\frac{\partial \phi}{\partial z} - c\frac{1}{2}\frac{\partial a^2}{\partial z}, \tag{3.6c}$$

where $N \equiv (n - n_0)/n_0$. We eliminate the $c\beta_z \partial\beta_z/\partial z$ term in Eq. (3.6c) since $\beta_z \ll 1$. It is convenient to write the equations in a co-moving coordinate system (ζ, τ) [44, 45], in which $\tau = t$ and $\zeta = z - ct$. Then the derivatives $\partial/\partial z$ and $\partial/\partial t$ are replaced by $\partial/\partial \zeta$ and $\partial/\partial \tau - c\partial/\partial \zeta$ respectively. If the laser pulse is sufficiently short, the field $\mathbf{a}$ and ϕ are expected to change very little during the transit time of the plasma through the pulse and the changes can be ignored in plasma reaction. Assuming that the laser envelop changes on a characteristic time scale $\tau_e \sim 2|n_0/n|(\omega/\omega_p)/\omega_p$, the quasistatic approximation (QSA) is applicable. In the QSA, $\partial/\partial \tau$ which determines the plasma response to the laser pulse are neglected in the plasma fluid equations . However, $\partial/\partial \tau$ is retained in the wave equation because it describes the evolution of the laser pulse [45, 32]. Thus for a short laser pulse, we can write Eq. (3.6a) to (3.6c) as

$$\frac{\partial^2 \phi}{\partial \zeta^2} = k_p^2 N, \tag{3.7a}$$

$$\frac{\partial}{\partial \zeta}(N - \beta_z) = 0, \tag{3.7b}$$

$$\frac{\partial \beta_z}{\partial \zeta} = -\frac{\partial \phi}{\partial \zeta} + \frac{1}{2}\frac{\partial a^2}{\partial \zeta}, \tag{3.7c}$$

Substituting Eq. (3.7a) and (3.7b) into Eq. (3.7c), we arrive at

$$\left(\frac{\partial^2}{\partial \zeta^2} + k_p^2\right)\phi = \frac{k_p^2}{2}a^2 \tag{3.8}$$

The solutions to the equation are easily calculated with the Green's function such that[46]

$$\phi \cong \frac{k_p}{2}\int_0^\zeta a^2(\zeta')\sin[k_p(\zeta' - \zeta)]d\zeta' \tag{3.9}$$

and the related axial field is obtained

$$\frac{E_z}{E_{wb}} = -\frac{1}{k_p}\frac{\partial \phi}{\partial \zeta} = \chi a_0^2$$

where $\chi = k_p/(2a_0^2) \int_0^\zeta a^2(\zeta') \cos[k_p(\zeta' - \zeta)]d\zeta'$ is the form factor which depends on the pulse shape. Here $E_{wb} \equiv mc\omega_p/e$ is the cold wavebreaking limit, characterizing the accelerating gradient G ($G = eE_z$) of the plasma accelerator. Since $k_p = \omega_p/c$, the solutions to Eq. (3.8) describe the plasma waves generated at the frequency ω_p and are valid far from wavebreaking, $E_z \ll E_{wb}$. Meanwhile the wakefields are generated sinusoidally and are efficient when the envelope scale length is on the order of the plasma wavelength $\lambda_p = 2\pi c/\omega_p$[46].

3.2.2   Nonlinear Regime

When the laser power is extremely high such that $a_0 \lesssim 1$, the plasma particle quiver motions become highly relativistic and a variety of nonlinear phenomena happens in the laser plasma interaction. It includes [45] (a) relativistic optical guiding of the laser beam[47, 48, 49], (b) the excitation of coherent radiation at harmonics of fundamental laser frequency, (c) the generation of large plasma wakefield, (d) frequency shift induced in the laser pulse by plasma waves[50, 51], (e) frequency amplification using an ionized front, and (f) the snow-plow acceleration[52, 53]. A full set of the fluid equations is required to describe the nonlinear phenomena. For the study of the generation of large plasma wakefield, we have the equations from Eq. (3.2a) to (3.2e) in terms of a and ϕ

$$\frac{\partial^2 \phi}{\partial z^2} = k_p^2 \left(\frac{n}{n_0} - 1\right), \tag{3.10a}$$

$$\frac{\partial n}{\partial t} + c\frac{\partial}{\partial z}(n\beta_z) = 0, \tag{3.10b}$$

$$\frac{d}{dt}(\gamma\boldsymbol{\beta}_\perp) = \frac{d\mathbf{a}}{dt}, \tag{3.10c}$$

$$\frac{d}{dt}(\gamma\beta_z) = c\frac{\partial\phi}{\partial z} - \frac{c}{2\gamma}\frac{\partial a^2}{\partial z}, \tag{3.10d}$$

$$\frac{d\gamma}{dt} = c\beta_z\frac{\partial\phi}{\partial z} + \frac{1}{2\gamma}\frac{\partial a^2}{\partial t}, \tag{3.10e}$$

with neglecting ω_c. From Eq. (3.10c), the conservation of transverse canonical momentum gives $\gamma\boldsymbol{\beta}_\perp = \mathbf{a}$ or $\gamma = (1 + a^2)^{1/2}/(1 - \beta_z^2)^{1/2}$. So the pulse is described by the wave equation of $\mathbf{a}$

$$\left[\frac{\partial^2}{\partial z^2} - \frac{1}{c^2}\frac{\partial^2}{\partial t^2}\right]\mathbf{a} = k_p^2\frac{n}{n_0}\boldsymbol{\beta}_\perp = k_p^2\frac{n}{n_0}\frac{\mathbf{a}}{\gamma}, \tag{3.11}$$

which leads to the dispersion relation in the relativistic regime

$$\omega^2 = k^2 c^2 + \frac{\omega_p^2}{\gamma} \tag{3.12}$$

by assuming a plane wave $a \propto \exp[i(kz - \omega t)]$ and $n = n_0$. We may combine this wave equation of $\mathbf{a}$ with the fluid equations to form a self-consistent equation set.

Insetting Eq. (3.10e) to Eq. (3.10d), we arrive at

$$\frac{d}{dt}(\gamma \beta_z - \gamma) = c(1 - \beta_z)\frac{\partial \phi}{\partial z} - \frac{1}{2\gamma}\left(c\frac{\partial}{\partial z} + \frac{\partial}{\partial t}\right)a^2. \tag{3.13}$$

It is convenient to transform Eq. (3.13) into the new coordinate system (ζ, τ), then the second term on the right hand side vanishes. Together with the Poisson equation and the continuity equation, we obtain the complete equations for ϕ in (ζ, τ) coordinate with QSA applied

$$\frac{\partial}{\partial \zeta}[n(1 - \beta_z)] = 0 \tag{3.14a}$$

$$\frac{\partial}{\partial \zeta}(\gamma \beta_z - \gamma + \phi) = 0 \tag{3.14b}$$

$$\frac{\partial^2 \phi}{\partial \zeta^2} = k_p^2\left[\frac{n}{n_0} - 1\right] \tag{3.14c}$$

in which Eq. (3.14c) expresses the potential of plasma wakefield. Equation (3.14a) and (3.14b) can be solved from the integration over ζ. Since the plasma keeps stationary until the driving pulse passes through, the boundary conditions for the two equations $\gamma = 1$, $n = n_0$ and $\beta_z = 0$ are applied and give the solutions

$$\gamma(1 - \beta_z) - \phi = 1, \tag{3.15a}$$

$$n(1 - \beta_z) = n_0. \tag{3.15b}$$

So that the ratio of n/n_0 is given,

$$\frac{n}{n_0} = \frac{1}{1 - \beta_z} = \frac{\gamma}{1 + \phi}, \tag{3.16}$$

and its quadratic form can be expressed as

$$\left(\frac{n}{n_0}\right)^2 = \left(\frac{1}{1 - \beta_z}\right)^2 = \frac{\gamma^2}{(1 + \phi)^2} = \frac{1 + a^2}{(1 - \beta_z)(1 + \beta_z)(1 + \phi)^2}$$

with $\gamma^2 = (1 + a^2)/(1 - \beta_z^2)$. Hence the differential equation of ϕ is written as

$$
\begin{aligned}
\frac{\partial^2 \phi}{\partial \zeta^2} &= k_p^2 \left[\frac{n}{n_0} - 1 \right] \\
&= k_p^2 \frac{\beta_z}{1 - \beta_z} \\
&= \frac{k_p^2}{2} \left[\frac{(1 + a^2)}{(1 + \phi)^2} - 1 \right]
\end{aligned}
\tag{3.17}
$$

and the plasma wakefield normalized by E_0 is obtained as $\partial \phi / \partial \zeta$. We then express the plasma quantities in terms of the fields a and ϕ as

$$
n/n_0 = 1 + \frac{1}{2}[(1 + a^2)/(1 + \phi)^2 - 1]
\tag{3.18a}
$$

$$
\gamma = [1 + a^2 + (1 + \phi)^2]/[2(1 + \phi)]
\tag{3.18b}
$$

$$
\beta_z = [1 + a^2 - (1 + \phi)^2]/[1 + a^2 + (1 + \phi)^2].
\tag{3.18c}
$$

Considering the weak field limit $\phi \ll 1$, Eq. (3.17) becomes

$$
\left(\frac{\partial^2}{\partial \zeta^2} + k_p^2 \right) \phi = \frac{k_p^2}{2} a^2
\tag{3.19}
$$

after taking the Taylor expansion to the first power. This equation reduces to that in linear case (Eq. (3.8)).

Since Eq. (3.17) is fully nonlinear, its analytical solution only exists for a circularly polarized laser pulse with a square pulse profile as the laser envelop, $a_L = a_0$ for $-L < \zeta < 0$ and $a_L = 0$ otherwise [54, 55, 56]. For simplification, we rewrite Eq. (3.17)

$$
\frac{\partial^2 \varphi}{\partial \zeta'^2} = \frac{1}{2} \left[\frac{\alpha^2}{\varphi^2} - 1 \right]
\tag{3.20}
$$

with $\varphi \equiv 1 + \phi$, $\zeta' \equiv k_p \zeta$ and $\alpha^2 \equiv 1 + a^2$. It can be integrated by first multiplying $\partial \varphi / \partial \zeta'$ on both sides

$$
\int \frac{\partial^2 \varphi}{\partial \zeta'^2} \frac{\partial \varphi}{\partial \zeta'} d\zeta' = \int \frac{1}{2} \left[\frac{\alpha^2}{\varphi^2} - 1 \right] \frac{\partial \varphi}{\partial \zeta'} d\zeta'.
$$

Then we get

$$
\left(\frac{\partial \varphi}{\partial \zeta'} \right)^2 = -\frac{\alpha^2}{\varphi} - \varphi + C_1,
\tag{3.21}
$$

where $C_1 = \alpha^2 + 1$ is the integration constant determined by the boundary condition that $\partial \varphi / \partial \zeta' = 0$ and $\varphi(\zeta') = 1$ at $\zeta' = 0$. Within the pulse that $-L < \zeta < 0$, the formal solution for $\varphi(\zeta')$ is [54, 55, 56]

$$
\zeta' = -2\alpha E(\theta_i, k_i) + 2 \left(\frac{(\alpha^2 - \varphi)(\varphi - 1)}{\varphi} \right)^{1/2},
\tag{3.22}
$$

27

with

$$\theta_i = \arcsin \left(\frac{\alpha^2(\varphi - 1)}{(\alpha^2 - 1)\varphi} \right)^{1/2}$$

and

$$k_i = \left(\frac{\alpha^2 - 1}{\alpha^2} \right)^{1/2}.$$

$E(\theta, k)$ here is the incomplete elliptic integration of the second kind and the second term on the right hand side of Eq. (3.22) indicates that φ is allowed to lie in the range $1 \leq \varphi \leq \alpha^2$. Thus the maximum $\varphi = \alpha^2$ occurs at $\zeta' = -2\alpha E(k_i)(E(k_i) = E(\pi/2, k_i))$ which gives the optimal pulse length

$$L_o = \frac{2}{k_p} \alpha E(k_i) \simeq \frac{\lambda_p}{2}$$

for $\alpha \sim 1$ $(k_i \ll 1$, $E(0) = \pi/2)$, and

$$L_o \simeq \frac{a_0}{\pi} \lambda$$

for $\alpha \gg 1$ $(k_i \sim 1$, $E(1) = 1)$. We notice when $\zeta' = -4\alpha E(k_i)$, $\varphi = 1$ implies $\phi = 0$. There is no wakefield excited behind the pulse.

Next with the laser pulse of length $L = L_o$, the equation of the plasma wakefield potential behind the pulse $(\zeta' < -L$ and $a = 0)$ is

$$\left(\frac{\partial \varphi}{\partial \zeta'} \right)^2 = -\frac{1}{\varphi} - \varphi + C_2, \tag{3.23}$$

where $C_2 = \alpha^2 + 1/\alpha^2$ is given from the boundary condition $(\partial \varphi/\partial \zeta')_{L_o} = 0$ and $\varphi(L_o) = \alpha^2$. The solution of φ is therefore

$$\zeta' = -k_p L_o - 2\alpha E(\theta_e, k_e) \tag{3.24}$$

with

$$\theta_e = \arcsin \left(\frac{\alpha^2(\alpha^2 - \varphi)}{\alpha^4 - 1} \right)^{1/2}$$

and

$$k_e = \left(\frac{\alpha^4 - 1}{\alpha^4} \right)^{1/2}.$$

Finally the axial electric field E_z (wakefield) related to φ is

$$\frac{E_z}{E_{wb}} \equiv \tilde{E}_z = -\frac{\partial \varphi}{\partial \zeta'},$$

Figure 3.2: Density variation $\delta n = n - n_0$ (dashed curve) and the axial electric field E_z normalized by E_0 (solid curve). The Gray shaded region is the Gaussian pulse, $a = a_0 \exp[-(\zeta + 5)^2/2^2]$ with $a_0 = 1.5$.

and the field is given by Eq. (3.23) such that

$$
\begin{aligned}
\tilde{E}_z^2 &= -\frac{1}{\varphi} - \varphi + \frac{1}{\alpha^2} + \alpha^2 \\
&= a_0^2 - \phi + \frac{1}{1 + a_0^2} - \frac{1}{1 + \phi}.
\end{aligned}
$$

Because $\tilde{E}_z$ is $\pi/2$ offset with ϕ, $\tilde{E}_z$ reaches the maximum when ϕ reaches 0. So that the maximum $\tilde{E}_z$ is

$$
\tilde{E}_{z\text{max}} = \frac{a_0^2}{\sqrt{1 + a_0^2}}. \tag{3.25}
$$

We notice that in highly nonlinear regime $a_0 \gg 1$, $\tilde{E}_{z\text{max}} \simeq a_0$, the accelerating gradient is linearly proportional to a_0, while in the linear regime $a_0 \ll 1$, $\tilde{E}_z \simeq a_0^2$, the accelerating gradient is proportional to the quadratic of a_0, which is consistent with the result in the linear regime Eq. (3.10).

If in general cases with arbitrary laser pulse shapes, numerical calculations are essential to solve the equation Eq. (3.17). Assuming a circularly polarized gaussian pulse, $a(\zeta) = a_0 \exp[-(\zeta - \zeta_0^2/2^2)]$, we plot the solution of Eq. (3.17) in
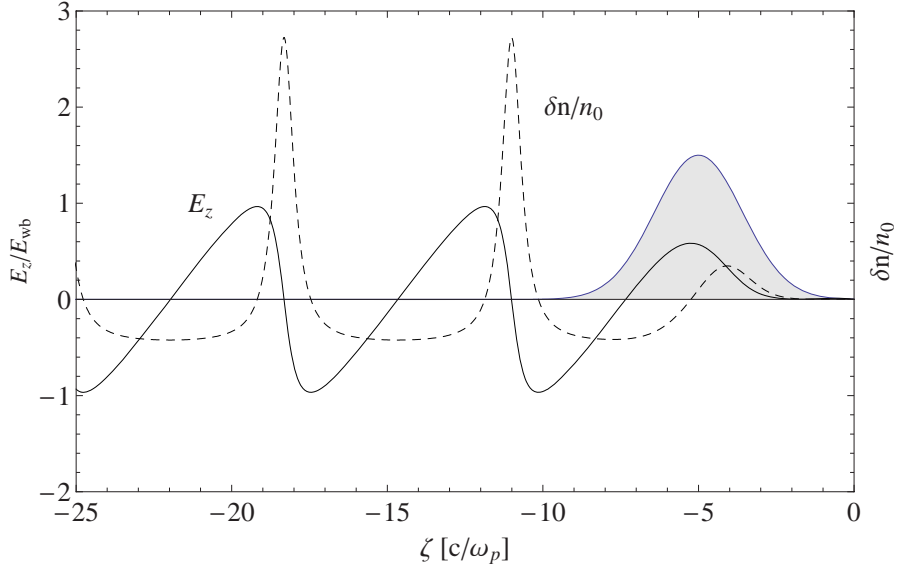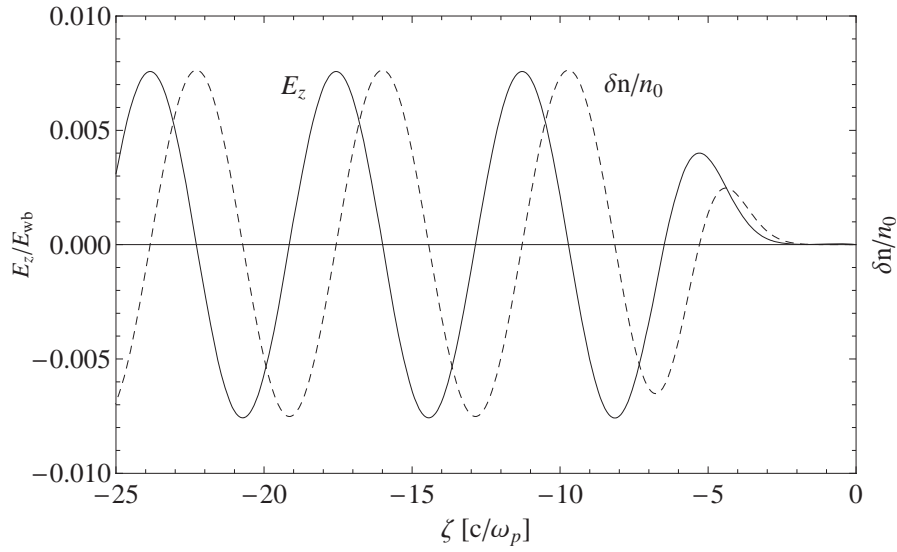
Figure 3.3: Density variation $\delta n = n - n_0$ (dashed curve) and the axial electric field E_z normalized by E_0 (solid curve) for Gaussian pulse $a = a_0 \exp[-(\zeta + 5)^2/2^2]$ with $a_0 = 0.1$.

Fig. 3.2 and 3.3 for $a_0 = 1.5$ and 0.1. Here the solid curve presents the plasma wakefield and the dashed curve presents the density perturbation $\delta n = n - n_0$. In the nonlinear case ($a_0 = 1.5$), the plasma wakefield exhibits a sawtooth-like shape and the plasma density piles up as a delta function. These were caused by the totally expelled electrons from a strong laser ponderomotive field. The plasma density piling up forms parallel charged plates which result in a linearly-varying electrostatic field between every two plates. As for $a_0 = 0.1$, the plot as shown in Fig. 3.3 is purely sinusoidal, consistent with the result in the linear regime.

Chapter 4

Plasma Wakefield Acceleration in Magnetized Plasma II
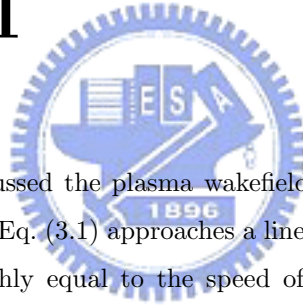
In Chap. 3 we have discussed the plasma wakefield under $\omega \gg \omega_c$. In which the dispersion relation in Eq. (3.1) approaches a linear relation of ω to k, whose phase velocities are roughly equal to the speed of light. It is appropriately utilized as the driving pulse for plasma wakefield excitation. But when $\omega < \omega_c$, the phase velocities of modes below the light curve (magnetowaves) are generally much less than c and vary with different k. Therefore a magnetowave pulse which is composed of different modes will quickly spread out during traveling. Nevertheless, we will show that, under a special condition (MPWA condition), the magnetowave will behaves like the light in vacuum and can be considered as a new type of driving pulses. In this chapter, we will focus on the magnetowave modes and establish the general theory of MPWA.

4.1 MPWA Condition

The idea of MPWA is first working on Alfven modes[26]. Alfven wave is a magnetic tension wave, only existing in magnetized plasma (medium wave) and having a very low phase velocity. However for an effective plasma accelerator,

31

here we instead concentrate on that whistler modes (the higher frequency mode). The dispersion relation of the whistler wave without considering the ion motion is given as

$$\omega^2 = k^2 c^2 + \frac{\omega_p^2}{1 - \omega_c/\omega} \,, \tag{4.1}$$

When the magnetic field is sufficiently strong such that $\omega_c/\omega \gg 1$ and $\omega_c \omega/\omega_p^2 \gg 1$, the second term on the right hand side of Eq. (4.1) is negligible. The whistler wave will have an approximately linear dispersion with phase velocity approaching c. It is instructive to combine the two linearity conditions into a chain inequality: $(\omega_c/\omega_p)^2 \gg \omega_c/\omega \gg 1$. Clearly, the range of ω compatible with this chain inequality increases with the ratio of ω_c/ω_p. In other words, for a larger ω_c/ω_p, the dispersion relation is approximately linear over a wider range of wavenumbers, as shown in Fig. 4.1. In the figure, there are three dispersion relation and phase velocity curves plotted with ω_c/ω_p equal to 1, 6 and 12 respectively. It is obvious that the curves behave likely to a normal light wave over a wider wavenumber range while the ratio ω_c/ω_p is sufficiently larger. Thus, when $\omega_c/\omega_p \gg 1$ is satisfied, the modes of whistler wave will contain coherent phase velocities which enables the whistler pulses to maintain their shape over a long distance, essential for an efficient plasma wakefield accelerator. Therefore, the requirement for MPWA is $\omega_c/\omega_p \gg 1$ where the dispersion relation is quasi-linear and the slope is near c. Such condition is referred to the "MPWA condition". In this chapter, the study of MPWA theory is under this condition.

4.2 Linear Theory

4.2.1 Ponderomotive Force

Once a whistler pulse is generated, the plasma wakefield will be sequentially excited by the ponderomotive force of the driving pulse. In Chap. 3, we have introduced the ponderomotive force as the gradient of the laser intensity. If ω_c/ω is not negligible, the effect from background magnetic field should be taken into account. The non-relativistic ponderomotive force in magnetized plasma has been studied extensively in the past [57, 58]. Assuming an external
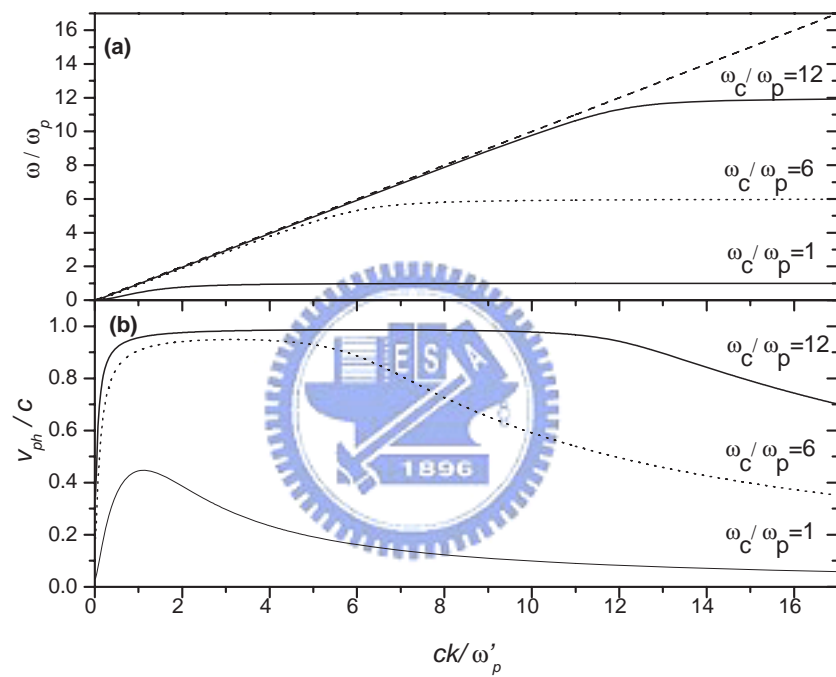
Figure 4.1: (a) Frequency and (b) phase velocity versus wavenumber for different magnetic field strengths. When $\omega_c/\omega_p \gg 1$, the dispersion relation is approximately linear over a wider range of wavenumbers with phase velocity approaching the speed of light.

magnetic field in z direction, according to [57], the longitudinal ponderomotive force acting on a unit volume is given as

$$f_z = \frac{\epsilon(\omega) - 1}{16\pi} \frac{\partial |\mathbf{E}_\perp|^2}{\partial z} + \frac{k}{16\pi\omega^2} \frac{\partial \left[\omega^2(\epsilon(\omega) - 1)\right]}{\partial \omega} \frac{\partial |\mathbf{E}_\perp|^2}{\partial t} - \frac{\partial p}{\partial z}, \qquad (4.2)$$

where p is the kinetic pressure and $\epsilon(\omega) = N^2(\omega)$. $N(\omega)$ is the refractive index for waves propagation along the magnetic field in plasma (for whistler wave $\epsilon = 1 - \omega_p^2/\omega(\omega - \omega_c)$). $\mathbf{E}_\perp$ is the slow-varying electric component of the wave $\tilde{\mathbf{E}}_\perp = 1/2(\mathbf{E}_\perp e^{-i\omega t} + c.c.)$. Because whistler wave is a right-handed circularly polarized wave, it's electric field can be written as $\mathbf{E}_\perp = E_\perp(1, i)e^{ikz}$. Substituting $\epsilon(\omega)$ and $\mathbf{E}_\perp$ into Eq. (4.2) and ignoring the effect of kinetic pressure, we arrive at

$$
\begin{aligned}
f_z &= \frac{1}{8\pi} \left[-\frac{\omega_p^2}{\omega(\omega - \omega_c)} \right] \frac{\partial E_\perp^2}{\partial z} + \frac{k\omega_p^2}{8\pi} \frac{\partial}{\partial \omega} (-\frac{\omega}{\omega - \omega_c}) \frac{\partial E_\perp^2}{\partial t}, \\
&= -\frac{1}{8\pi} \frac{\omega_p^2}{\omega(\omega - \omega_c)} \frac{\partial E_\perp^2}{\partial z} + \frac{k\omega_p^2}{8\pi\omega^2} \left[\frac{\omega_c}{(\omega - \omega_c)^2} \right] \frac{\partial E_\perp^2}{\partial t}, \\
&= -\frac{\omega_p^2}{8\pi} \left(\partial_z - \frac{k\omega_c}{\omega(\omega - \omega_c)} \partial_t \right) \frac{E_\perp^2}{\omega(\omega - \omega_c)}.
\end{aligned}
\qquad (4.3)
$$

When taking the $\omega_c/\omega = 0$ limit, the expression (4.3) reduces to

$$f_z = -\frac{\omega_p^2}{8\pi} \frac{E_\perp^2}{\omega^2} = -mc^2 n_0 \frac{\partial}{\partial z}(\frac{a^2}{2})$$

which is the ponderomotive force in unmagnetized case.

4.2.2 Linear Formulation

With the ponderomotive force given above, we are able to calculate the plasma wakefield driven by the whistler pulse. Substituting Eq. (4.3) into the second term of the right hand side of Eq. (3.2d), the linear plasma wakefield can be formulated with $\gamma \sim 1$ through the set of 1-D fluid equations (Eq. (3.2a),(3.2b) and (3.2d))

$$\frac{\partial^2 \phi}{\partial z^2} = k_p^2 \left(\frac{n}{n_0} - 1 \right) \qquad (4.4a)$$

$$\frac{\partial n}{\partial t} + c\frac{\partial}{\partial z}(n\beta_z) = 0 \qquad (4.4b)$$

$$\frac{\partial \beta_z}{\partial t} = c\frac{\partial \phi}{\partial z} + \frac{f_z}{cmn_0}. \qquad (4.4c)$$

Under the MPWA condition where $\omega_c/\omega_p \gg 1$, the phase velocity $v_{ph} = \omega/k \sim c$ and the whistler pulse with central frequency ω would roughly travel at a group velocity $v_g \sim v_{ph} \sim c$. So that we can still rewrite the fluid equations in terms of the coordinate (ζ, τ) where $\zeta = z - v_g t = z - ct$ and $\tau = t$. Applying the QSA, we rearrange these equations as

$$\frac{\partial}{\partial\zeta}N - \frac{\partial}{\partial\zeta}\beta_z = 0, \tag{4.5}$$

$$\frac{\partial}{\partial\zeta}\beta_z = -\frac{\partial\phi}{\partial\zeta} + \frac{1}{2}\left(1 + \frac{k\omega_c c}{\omega(\omega - \omega_c)}\right)\frac{e^2}{m^2 c^2 \omega(\omega - \omega_c)}\frac{\partial}{\partial\zeta}E_\perp^2$$

$$= -\frac{\partial}{\partial\zeta}\phi + \frac{1}{2}\frac{e^2}{m^2 c^2 (\omega - \omega_c)^2}\frac{\partial}{\partial\zeta}E_\perp^2, \tag{4.6}$$

$$\frac{\partial^2}{\partial\zeta^2}\phi = k_p^2 N, \tag{4.7}$$

where $N \equiv (n - n_0)/n_0$. Combining equations Eq. (4.5), (4.7) and (4.6), we obtain the equation for ϕ

$$(\partial_\zeta^2 + k_p^2)\phi = \frac{1}{2}\frac{k_p^2 e^2}{m^2 c^2 (\omega - \omega_c)^2}E_\perp^2$$

$$= \frac{k_p^2}{2}\frac{a^2}{(1 - \omega_c/\omega)^2} \tag{4.8}$$

From Eq. (4.8), we notice that the denominator of the source term is quadratic so that this equation is applicable to waves with frequency both upper (R wave) and lower (whistler wave) branches. However there is a singularity for $\omega = \omega_c$ in which the plasma will resonate with the cyclotron frequency ω_c and eventually get heated. Therefore the wave propagation is forbidden. When ω is extremely high compared to ω_c, the effect of ω_c can be ignored and Eq. (4.8) reduces to the normal laser plasma wakefield equation in Eq. (3.8). With a fixed pulse frequency, the wakefield amplitude increases as the background magnetic field strength increases[43]. But for a whistler wave which has a frequency smaller than ω_c, the plasma wakefield amplitude decreases as the magnetic field increases.

We can solve the analytic solution of Eq. (4.8) readily via the Green's function with the boundary conditions $\phi(\zeta \to \infty) = 0$ and $\partial\phi(\zeta \to \infty)/\partial\zeta = 0$ applied. The solution reads

$$\phi(\zeta) = \frac{k_p}{2}\frac{a_0^2}{(1 - \omega_c/\omega)^2}\int_\zeta^\infty d\zeta'\frac{a^2(\zeta')}{a_0^2}\sin[k_p(\zeta' - \zeta)]. \tag{4.9}$$

Hence

$$\frac{E_z}{E_{wb}} = \frac{1}{k_p}\frac{\partial\phi}{\partial\zeta} = -\frac{k_p}{2}\frac{a_0^2}{(1-\omega_c/\omega_c)^2}\int_\zeta^\infty d\zeta' \frac{a^2(\zeta')}{a_0^2}(\zeta')\cos[k_p(\zeta-\zeta')]$$

$$= \chi(\zeta)\frac{a_0^2}{(1-\omega_c/\omega)^2}, \qquad\qquad (4.10)$$

with

$$\chi(\zeta) = \frac{k_p}{2a_0^2}\int_\zeta^\infty d\zeta' a^2(\zeta')\cos[k_p(\zeta-\zeta')]. \qquad\qquad (4.11)$$

Compared this result to that of the unmagnetized case in Eq. (3.10), $E_z(\zeta)$ has a multiplied factor $1/(1-\omega_c/\omega)^2$ from the influence of background magnetic field. We may have an extra gain in the accelerating gradient with ω_c/ω approaching unity. For a circularly polarized Gaussian wavepacket of width σ, i.e., $E_\perp^2 = E_{\perp 0}^2\exp(-\zeta^2/\sigma^2)$, the factor $\chi(\zeta)$ can be calculated analytically as following [59]

$$\chi(\zeta) = \frac{\sqrt{\pi}}{2}k_p\sigma\exp(-k_p^2\sigma^2/2)\cos(k_p\zeta). \qquad\qquad (4.12)$$

4.3 Nonlinear Theory

4.3.1 MPWA Condition in Relativistic Regime

In astrophysical environment, the amplitude of magnetowave could be very intense and the plasma quiver motions become highly relativistic. In turn, the electron effective mass will be increased by a factor $\gamma = (1-\beta_\perp^2-\beta_z^2)^{-1/2}$, causes the dispersion relation of whistler wave as

$$\omega^2 = c^2k^2 + \frac{\omega_p^2/\gamma}{1-\omega_c/\gamma\omega} = c^2k^2 + \frac{\omega_p'^2}{1-\omega_c'/\omega} \qquad\qquad (4.13)$$

in which $\omega_p' \equiv \omega_p/\sqrt{\gamma}$ and $\omega_c' \equiv \omega_c/\gamma$. To ensure the linear dispersion relation with slope $\sim c$, the MPWA condition in the nonlinear regime requires $\omega_c'/\omega_p' \gg 1$ or $\omega_c/\omega_p \gg \sqrt{\gamma}$.

4.3.2 Nonlinear Formulation

Considering the γ factor, the ponderomotive force from whistler waves in relativistic regime becomes more complicated. It is not intuitive to write down the equations involving the ponderomotive force. So that we can only treat the full

fluid equations (Eq. (3.2a) to (3.2e)) such that,

$$\frac{\partial^2 \phi}{\partial z^2} = k_p^2 \left(\frac{n}{n_0} - 1 \right)$$

$$\frac{\partial n}{\partial t} + c \frac{\partial}{\partial z}(n\beta_z) = 0,$$

$$\frac{d}{dt}(\gamma \beta_\perp) = \frac{da}{dt} - i\omega_c \beta_\perp,$$

$$\frac{d}{dt}(\gamma \beta_z) = c \frac{\partial \phi}{\partial z} - \frac{e}{mc}(\beta_x B_y - \beta_y B_x),$$

$$\frac{d\gamma}{dt} = -\frac{e}{mc}(\beta_x E_x + \beta_y E_y + \beta_z E_z).$$

Transforming the above equations into the (ζ, τ) coordinate and assuming the QSA condition, we obtain

$$\frac{\partial^2 \phi}{\partial \zeta^2} = k_p^2(\frac{n}{n_0} - 1), \tag{4.15a}$$

$$\frac{\partial}{\partial \zeta}[n(1 - \beta_z)] = 0, \tag{4.15b}$$

$$\frac{\partial}{\partial \zeta}(\gamma \beta_\perp - a) = i\frac{\omega_c}{c}\frac{\beta_\perp}{1 - \beta_z}, \tag{4.15c}$$

$$-(1 - \beta_z)\frac{\partial}{\partial \zeta}\gamma \beta_z = \frac{\partial \phi}{\partial \zeta} - \frac{e}{mc^2}(\beta_x B_y - \beta_y B_x) \tag{4.15d}$$

$$-(1 - \beta_z)\frac{\partial \gamma}{\partial \zeta} = \beta_z\frac{\partial \phi}{\partial \zeta} - \frac{e}{mc^2}(\beta_x E_x + \beta_y E_y) \tag{4.15e}$$

in which the total time derivative d/dt is replaced by $-c(1-\beta_z)\partial/\partial\zeta$. Under the MPWA condition where $v_{ph} \sim c$, the Maxwell's equation $\nabla \times \boldsymbol{E} = -(1/c)\partial \boldsymbol{B}/\partial t$ claims

$$\partial_\zeta E_x = \partial_\zeta B_y$$

$$\partial_\zeta E_y = -\partial_\zeta B_x.$$

Hence all B components in Eq. (4.15d) can be replaced by the E components,

$$-(1 - \beta_z)\frac{\partial}{\partial \zeta}(\gamma \beta_z) = \frac{\partial \phi}{\partial \zeta} - \frac{e}{mc^2}(\beta_x E_x - \beta_y E_y). \tag{4.16}$$

Substituting Eq. (4.15e) into Eq. (4.16), we obtain

$$\frac{\partial}{\partial \zeta}(\phi - \gamma(1 - \beta_z)) = 0, \tag{4.17}$$

and together with Eq. (4.15b),

$$\phi - \gamma(1 - \beta_z) = -1, \tag{4.18a}$$

$$n(1 - \beta_z) = n_0 \tag{4.18b}$$

37

after integrating over ζ and applying the boundary condition. They are in the same forms as those in the unmagnetized plasma case (Eq. (3.15a) and (3.15b)) [45]. The main difference between the two cases is on the Lorentz factor γ which defines $(1 - \beta_\perp^2 - \beta_z^2)^{-1/2}$.

We can solve the transverse fluid velocity $\beta_\perp$ directly from Eq. (4.15c). Under the QSA, the transverse $\beta_\perp$ is obtained as

$$\beta_\perp = \frac{a}{|\gamma - \frac{\omega_c}{\omega(1 - \beta_z)}|}. \tag{4.19}$$

We note that in magnetized plasma the condition for non-relativistic case where $\gamma \sim 1$, $\beta_\perp \ll 1$ and $\beta_z \ll 1$ requires $a \ll \omega_c/\omega - 1$ ($a \ll 1$ for unmagnetized plasma). Thus, the system could be still in non-relativistic regime even with $a_0 > 1$ so long as ω_c/ω is much greater than a_0.

With $\beta_\perp$ solved in terms of a (Eq. (4.19)), we have

$$\gamma^2 \beta_\perp^2 = \gamma^2 (1 - \beta_z^2) - 1 = \frac{a^2}{\left(1 - \frac{\omega_c}{\omega\gamma(1 - \beta_z)}\right)^2} \tag{4.20}$$

Therefore by combining Eq. (4.20), (4.18a) and (4.18b) , the Poisson equation for the plasma wakefield (Eq. (4.15a)) becomes

$$\frac{\partial^2 \phi}{\partial \zeta^2} = \frac{k_p^2}{2} \left[\left(\frac{a^2}{(1 - \frac{\omega_c}{\omega(1 + \phi)})^2} + 1 \right) \frac{1}{(1 + \phi)^2} - 1 \right], \tag{4.21}$$

which is also valid in all frequency ranges (Appendix B). We discuss the equation in two limits. For $\omega \gg \omega_c$ ($\omega_c/\omega \to 0$), this equation reduces to that in the unmagnetized plasma (Eq. (3.17)) [45]; and for $\phi \ll 1$, it is easy to show that Eq. (4.21) returns to the non-relativistic MPWA equation in Eq. (4.8).

4.3.3 Numerical Results

Since Eq. (4.21) is fully nonlinear, there is no analytical solution found to the equation. Thus the only way to solve the equation is numerical calculation. Assuming $\omega_c/\omega = 5$, we plot the solutions of plasma wakefield in Figs. 4.2 and 4.3 with $a_0 = 1$ and $a_0 = 4$ respectively. The plasma is driven by the whistler gaussian pulse with a width $\sqrt{2}(c/\omega_p)$. The solid curves denote the plasma
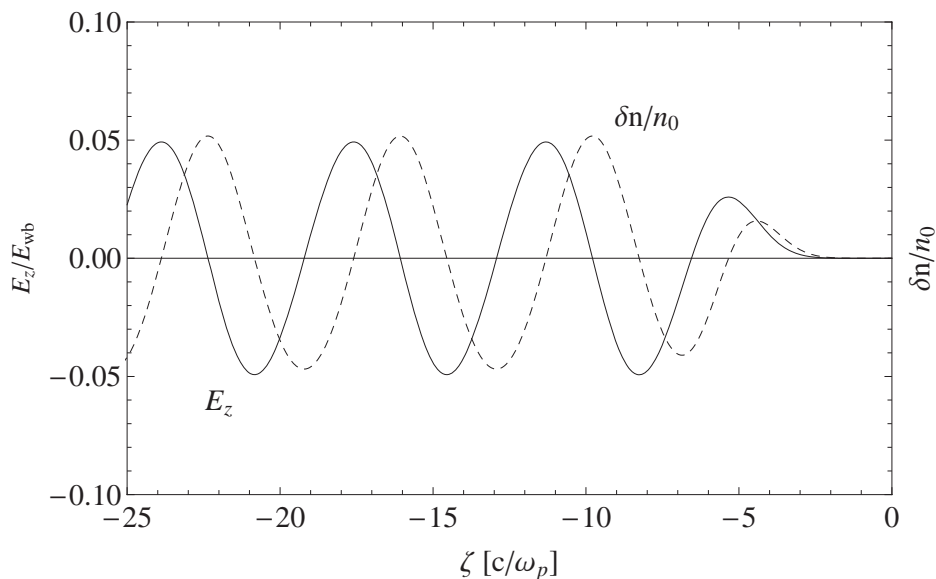
Figure 4.2: Density variation $\delta n/n$ and axial field E_z for whistler gaussian pulse located at $\zeta = -5(c/\omega_p)$ and $a_0 = 1$.

wakefield amplitude normalized by E_{wb} and the dashed curves superimposed in the figures are the plasma density variation $\delta n/n = n/n_0 - 1$ in terms of fields a and ϕ derived from Eq. (4.18b), (4.18a) and (4.19). In $a_0 = 1$ case, where $a_0 < \omega_c/\omega - 1 = 4$, the plasma wakefield behaves like sinusoidal. But in the other case, the plasma starts piling up and the associated axial E_z (the plasma wakefield) becomes sawtooth-like when $a_0 = 4$.

4.4 Limitation of MPWA

By looking at the successful derivation of MPWA equation, we note that the right hand side of Eq. (4.21) becomes singular as $1 + \phi \to \omega_c/\omega$. In such a limit, both the slope of E_z and the plasma density become infinite, which indicates the occurrence of wavebreaking. Beyond this point, the development of plasma waves is expected to become turbulent due to the instability, and our fluid equation analysis will break down. The electric field is expected to remain finite since the amplitude of a relativistic plasma wave is proportional to $\sqrt{\gamma} = (1 - \beta_{z,\text{max}}^2)^{-1/4}$ where $\beta_{z,\text{max}}$ is the maximum electron velocity in
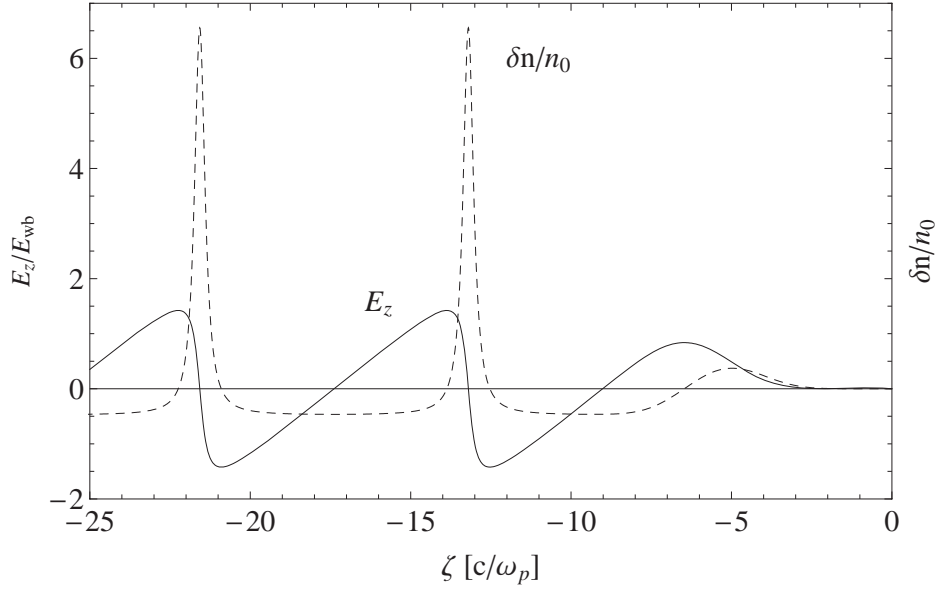
Figure 4.3: Density variation $\delta n/n$ and axial field E_z for whistler gaussian pulse located at $\zeta = -5(c/\omega_p)$ and $a_0 = 4$.

the wave. The above infinite-density situation would not occur if the strength parameter a_0 is smaller than an upper bound determined by the ratio ω_c/ω and the shape of the whistler pulse[60].

In order to study the sensitivity of $\omega_c/\omega \equiv b$ to the limit of a_0, we compare three results of Eq. (4.21) corresponding to $b = 0$, $0 < b < 1$ and $b > 1$.

4.4.1 Three Cases

1. $b = 0$

When $b = 0$, there is no background magnetic field, Eq. (4.21) can be reduced to

$$\frac{\partial^2 \varphi}{\partial \zeta'^2} = \frac{1}{2} \left[\frac{\alpha^2}{\varphi^2} - 1 \right], \tag{4.22}$$

where $\varphi \equiv 1 + \phi$, $\alpha^2 \equiv 1 + a_0^2$ and $\zeta' \equiv k_p \zeta$. Assuming a circularly polarized square driving pulse with $a(\zeta) = a_0$ for $-L \leq \zeta \leq 0$, and $a(\zeta) = 0$ elsewhere, the equation within the pulse is integrated by multiplying $\partial \varphi/\partial \zeta'$ on both sides

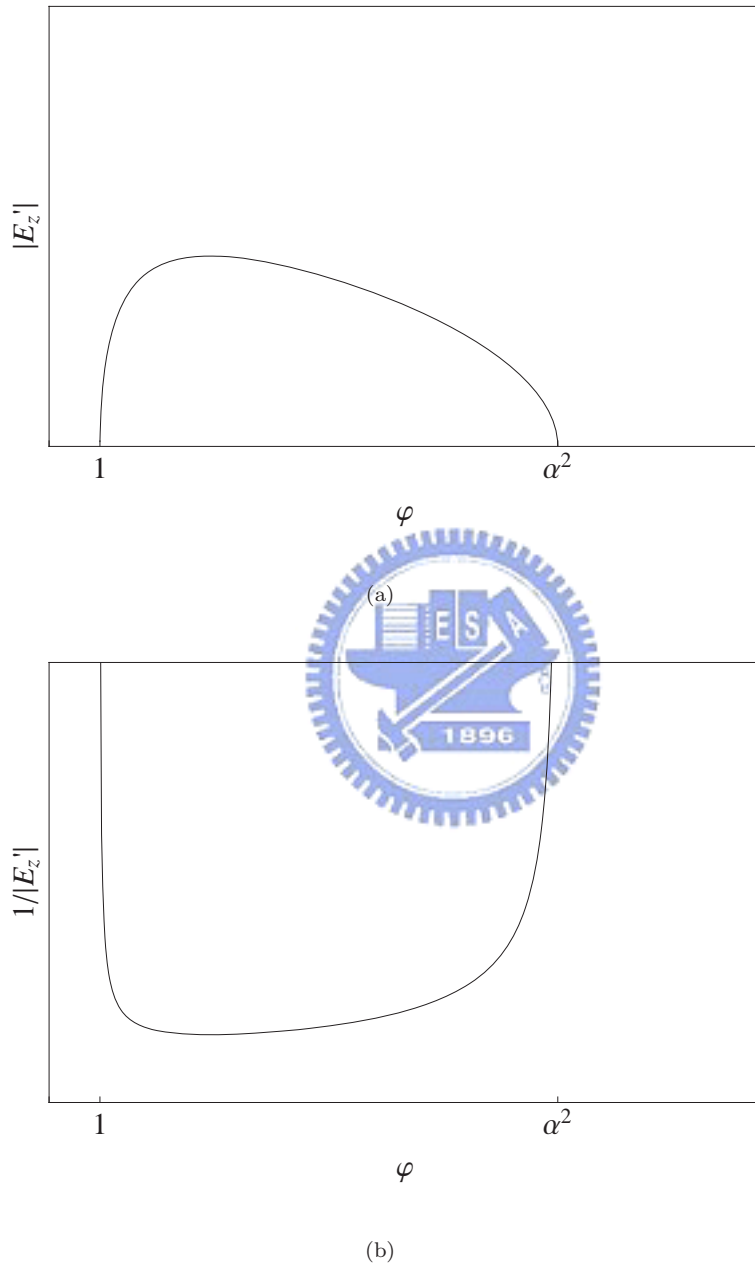Figure 4.4: The plots of (a) $|E_z'|$ and (b) $|1/E_z'|$ versus φ with $b = 0$ and $a_0 = 3$, where $\varphi \equiv 1 + \phi$ and $\alpha^2 \equiv 1 + a_0^2$.

of Eq. (4.22). Subjecting the boundary conditions $\varphi(\zeta') = 1$ and $(\partial\varphi/\partial\zeta') = 0$ at $\zeta' = 0$ to the equation, we arrive at

$$\left(\frac{\partial\varphi}{\partial\zeta'}\right)^2 \equiv E_z'^2 \quad = \quad -\frac{\alpha^2}{\varphi} - \varphi + \alpha^2 + 1, \tag{4.23}$$

$$= \quad (\alpha^2 - \varphi)\left(1 - \frac{1}{\varphi}\right) \geq 0, \tag{4.24}$$

where $E_z' \equiv E_z/E_{wb}$. The quadratic E_z' on the left hand side of Eq. (4.24) restricts the product of $\alpha^2 - \varphi$ and $1 - 1/\varphi$ to be positive. Hence the two terms have to be both positive to satisfy the inequality and φ is constrained to be $1 \leq \varphi \leq \alpha^2$. Another possible solution to the inequality with both terms negative is ruled out because no overlapped φ for $\varphi < 1$ and $\varphi > \alpha^2$ exists. Thus from the inequality solution of φ, the maximum φ is α^2 at an optimized length where $\partial\varphi/\partial\zeta' = 0$. There is no upper bound for α and neither is the plasma wakefield potential. We can clearly show that in the plots of $|E_z'|$ and $|1/E_z'|$ versus φ (Fig. 4.4(a) and Fig. 4.4(a)).

2. $0 < b < 1$

Following the same strategy, we find $E_z'^2$ from the integration of Eq. (4.21) in $0 < b < 1$ case,

$$E_z'^2 \quad = \quad -\frac{a_0^2}{\varphi - b} - \frac{1}{\varphi} - \varphi + \frac{a_0^2}{1 - b} + 2, \tag{4.25}$$

$$= \quad (\varphi - 1)\left[\frac{a_0^2}{(b - \varphi)(b - 1)} + \frac{1}{\varphi} - 1\right] \geq 0. \tag{4.26}$$

Again, in order to satisfy the inequality, one requires $a_0^2/(b-\varphi)(b-1) + 1/\varphi - 1 \geq 0$. It is easy to show that, for $b < 1$, the range of φ is solved as

$$1 \leq \varphi \leq \frac{\frac{a_0^2}{1-b} + 1 + b + \sqrt{(\frac{a_0^2}{1-b} + 1 + b)^2 - 4b}}{2}, \tag{4.27}$$

where the square root is always real because of the reason, $(\frac{a_0^2}{1-b}+1+b)^2-4b > (\frac{a_0^2}{1-b})^2 + (1-b)^2 > 0$. Therefore the maximum of φ is determined by a_0 and b and no upper bound on a_0 exists. From Eq. (4.27), when B_0 (or b) increases, the maximum φ as well as the maximum E_z also enhance accordingly, consistent with the conclusion by P. K. Shukla in Ref. of [43].
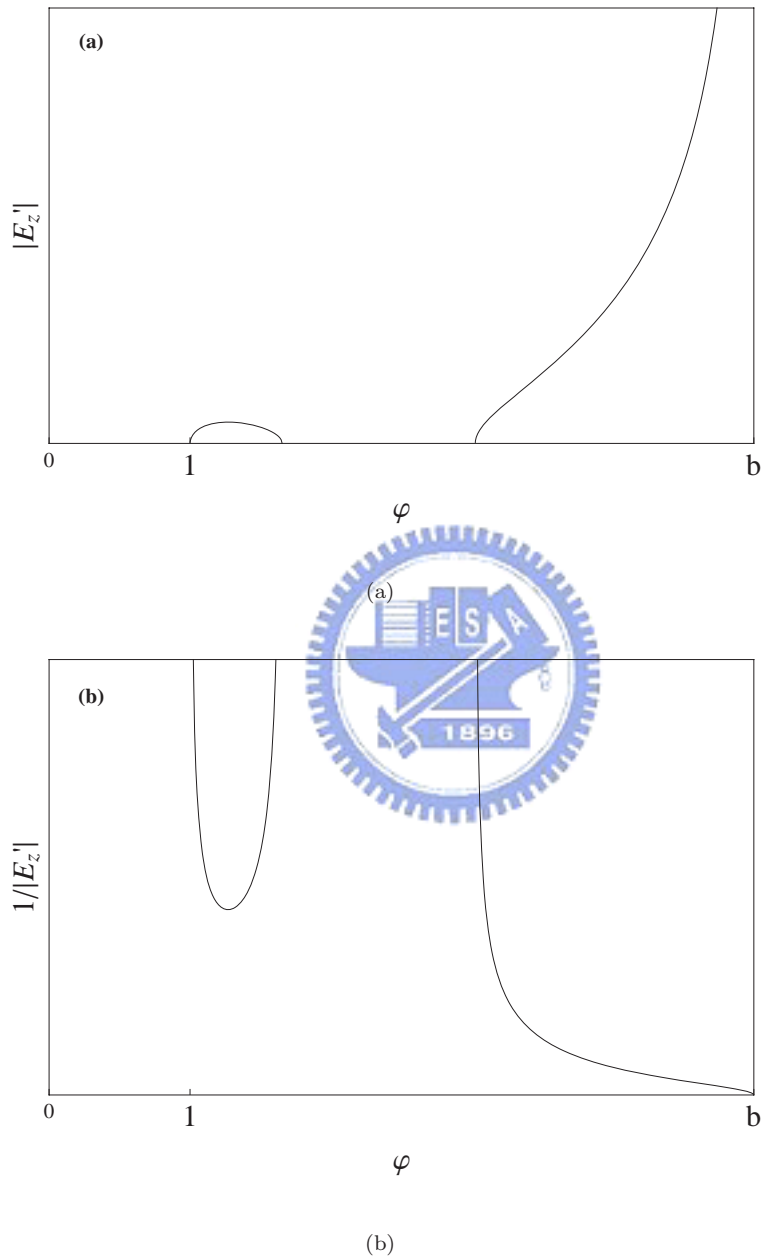
(a)

(b)

Figure 4.5: The plots of (a) $|E_z'|$ and (b) $|1/E_z'|$ versus φ with $b = 5$ and $a_0 = 2.3$ $(< \sqrt{b-1}(\sqrt{b}-1) = 2.47)$.

3. $b > 1$

Finally we treat the MPWA case which has $b > 1$. Unlike the two previous cases, the range of φ is solved as

$$b > \varphi \geq \frac{\frac{a_0^2}{1-b} + 1 + b + \sqrt{(\frac{a_0^2}{1-b} + 1 + b)^2 - 4b}}{2} \tag{4.28}$$

or equivalently

$$1 \leq \varphi \leq \frac{\frac{a_0^2}{1-b} + 1 + b - \sqrt{(\frac{a_0^2}{1-b} + 1 + b)^2 - 4b}}{2}. \tag{4.29}$$

Mathematically, if the square root $\sqrt{(a_0^2/(1-b) + 1 + b)^2 - 4b}$ in the numerator is real, then there exists two solutions for the range of φ. It can be traced back to the formula of $\beta_\perp$ (Eq. (4.19)) in which a small a_0 allows two possible solutions for $\beta_\perp$s, i.e., $\beta_\perp \ll 1$ or $\beta_\perp \sim 1$ when $\gamma \to b/(1 - \beta_z)$. Fortunately, the boundary conditions, $\beta_\perp(0) = \beta_z(0) = 0$ and $\gamma(0) = 1$, help us to eliminate the non-physical solution $\beta_\perp \sim 1$. Figure 4.5 is the plots of $|E_z{}'|$ and $|1/E_z{}'|$ versus φ, clearly exhibiting the two branches of φ. We can see that in the left branch E_z' is bounded by Eq. (4.29), similar to Fig. 4.4, and in right branch E_z' will diverge even if a_0 is small.

However once the square root $\sqrt{(a_0^2/(1-b) + 1 + b)^2 - 4b}$ is not real, the φ is no longer determined by the combination of a_0 and b, but only bounded by 1 and b, as shown in Fig. 4.6. The two branches have merged together. In this situation, there is no physical solution. As a result the magnetowave induced plasma wakefield driven by a constant pulses will has an upper limit on a_0 such that

$$(\frac{a_0^2}{1-b} + 1 + b)^2 > 4b, \text{ or } a_0 < (\sqrt{b} - 1)\sqrt{b - 1}. \tag{4.30}$$

4.4.2 Maximum of MPWA

When $b \gg 1$, the upper limit of a_0 is linear;y proportional to b. Beyond the upper limit of a_0, where $a_{0\max} = (\sqrt{b} - 1)\sqrt{b - 1}$, the plasma becomes dramatically turbulent and no plasma wake can be generated in this case. Therefore the plasma wakefield amplitude would also have a maximum, determined by $a_{0\max}$.

(a)
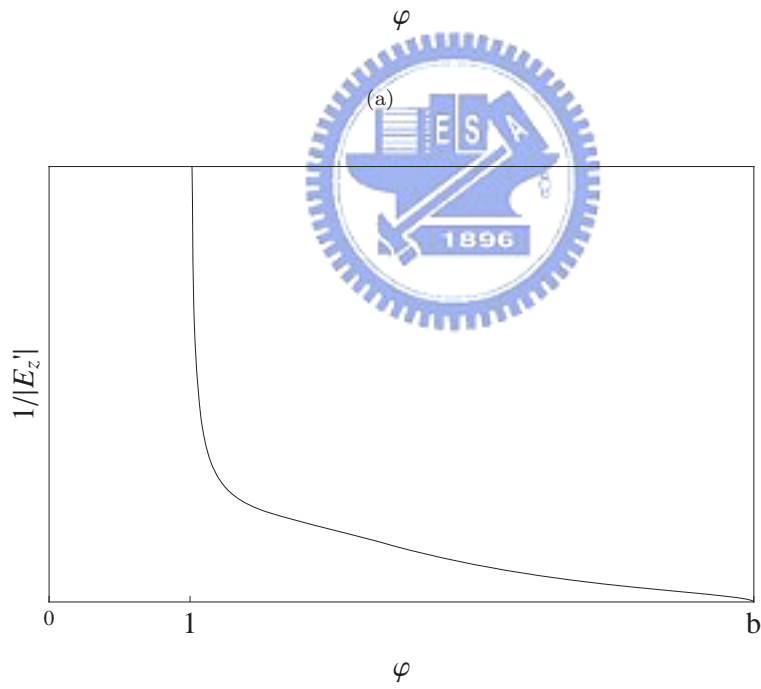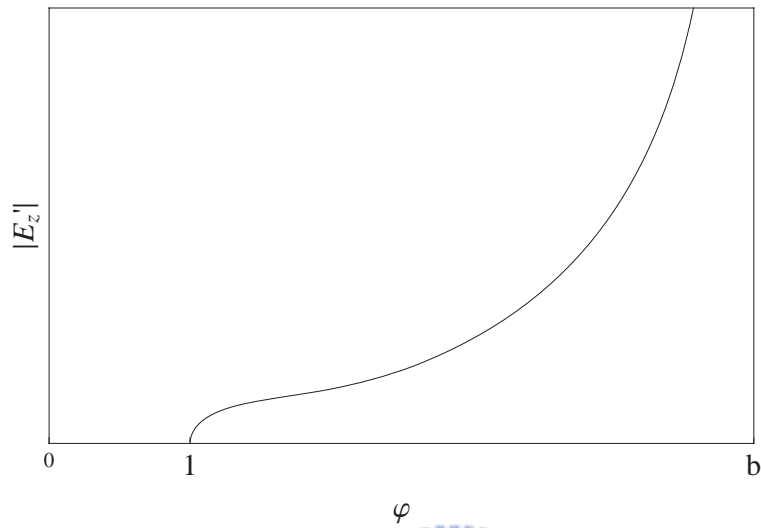
(b)

Figure 4.6: The plots of (a) $|E'_z|$ and (b) $|1/E'_z|$ versus φ with $b = 5$ and $a_0 = 3$ $(> \sqrt{b-1}(\sqrt{b}-1) = 2.47)$.

45

In our analysis, we only take the square driving pulse as the example. Nevertheless, we can still predict the maximum wakefield amplitude in real cases from the estimation. Assuming $b = 20$ and $a_0 = 15.1 (< (\sqrt{b} - 1)\sqrt{b - 1} = 15.135)$ of the pulse, the maximum of φ is calculated as 4 from Eq. (4.29) at an optimized distance with $\partial\varphi/\partial\zeta' = 0$. From the equation that describing the plasma wakefield behind the pulse,

$$\frac{\partial^2\varphi}{\partial\zeta'^2} = \frac{1}{2}\left(\frac{1}{\varphi^2} - 1\right),$$

we have

$$\left(\frac{\partial\varphi}{\partial\zeta'}\right)^2 = -\frac{1}{\varphi} - \varphi + C_1$$

with C_1 an integration constant, obtained from the boundary condition $\partial\varphi/\partial\zeta' = 0 = -1/\varphi_{max} - \varphi_{max} + C_1$. Hence $E_z'^2 = -1/\varphi - \varphi + 1/\varphi_{max} + \varphi_{max}$. The maximum of E_z' occurs at $\varphi = 1$ or $\phi = 0$. So that

$$E_{zmax}' = E_{zmax}/E_{wb} = \sqrt{-1 - 1 + 1/4 + 4} = 1.5$$

Since the square driving pulse could deposit most of the energy into the plasma, we may expect a higher upper bound on a_0 for a realistic driving pulse profile and therefor a high maximum E_z. As a conclusion, we may estimate E_{zmax} of MPWA to be $(1 - 10)E_{wb}$.

Chapter 5

Particle in Cell Simulation

5.1 Introduction

We have analytically established the general MPWA mechanism in the previous chapter. In order to confirm the theoretical model of the acceleration gradient ($G = eE_z$) and investigate the dynamical behavior, a self-consistent study of MPWA process via computer simulation is necessary. Generally, there are three schemes classified for the plasma simulation: the fluid scheme, the particle scheme and the hybrid. The particle scheme integrates the Newton-Lorentz equations of motion

$$\frac{d\mathbf{r}}{dt} = \mathbf{v}, \tag{5.1a}$$

$$\frac{d\gamma\mathbf{v}}{dt} = \frac{e}{m}\left(\mathbf{E} + \frac{\mathbf{v}}{c} \times \mathbf{B}\right) \tag{5.1b}$$

in the self-consistent electric and magnetic field configuration determined by the solution to Maxwells equation. In our work, we conducted the particle simulation using particle-in-cell(PIC) method which uses the particle scheme and is widely performed in plasma simulation.

Historically the roots of PIC method can be traced back to the self- consistent calculation performed by Buneman[61] and Dawson[62] in the late 1950s [63]. It is not until 1970s that the PIC scheme was formalized and coded. In the following decade, the class textbooks were published by Birdsall and Langdon[64], and Hockney and Eastwood[65]. Figure 5.1 shows the general flow chart of

PIC algorithm [64]. In PIC simulation, each single particle represents many particles to simulate the real plasma. Therefore each particle is introduced a finite-size to suppress the short range coulomb force between two particles[66]. The simulation box was divided into meshes. As an initial condition, particles are defined in continuum space in both position and velocity which are offset by half time step for the leap-frog scheme. The fields are defined at discrete locations in space. Particle density ρ and current density $\mathbf{J}$ for the field equations are accumulated from the particle locations to the nearby discrete mesh locations. Then the fields are advanced one time step from the updated rho and $\mathbf{J}$. In sequence particles experience the field force interpolated from the discrete grids and then update their locations and velocities. Next the boundary conditions for particles are applied and the time step loop repeats iteration.

In the early days before the PIC method was developed, the particle simulation of plasma calculated the Coulomb force between every two particles, taking an N^2 operations for N particles. It becomes extremely inefficient when N is large. Later on, the PIC method made a great improvement of scaling in N by imposing the computational meshes on which to compute Poisson equation [63]. Therefore, the PIC method is popularly applied nowadays in the simulation of plasma devices, plasma accelerators, space plasma and astrophysical jets., etc. for its accuracy and efficiency.

5.2 The "em1da" Code

For our work, we used a PIC code called "em1da", originally composed by R.Sydora [67] for 1 and 1/2 dimensional and fully relativistic electromagnetic problems. In this code, the Heaviside-Lorentz unit system was set up in order to eliminate the 4π factor in electromagnetism for convenience. I will discuss the details of the code in the following sections.

5.2.1 Simulation Unit

Usually computer simulations deal with dimensionless quantities for simplification. Some basic physical quantities, such as time, length and mass are normalized by the real plasma quantities. In em1da, the charge and mass of a
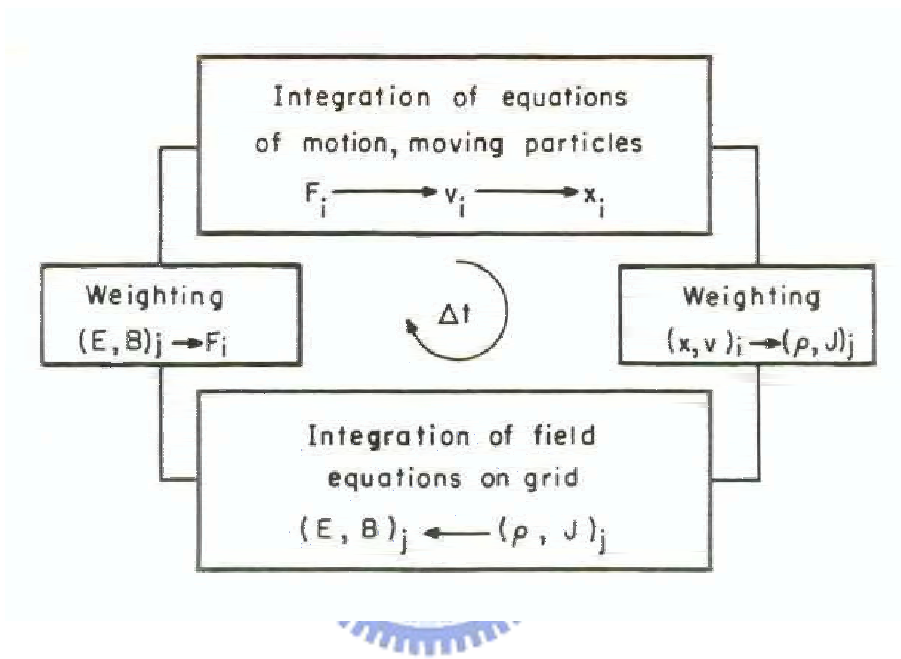
Figure 5.1: The general flow chart for the PIC scheme.

particle are normalized by the electron charge and electron mass and the time is normalized by a single plasma period ($t = \omega_p t_r$, where the subscript r means the real quantity). Accordingly the frequencies are normalized by the plasma frequency ω_p which is set to be 1. To find the scaling law of the field strength E and B, we may rewrite the Poisson equation as

$$\nabla \cdot E_r = e\delta n.$$

and then multiply e/m and divide by ω_p^2 on the both sides

$$\nabla \cdot \left(\frac{eE_r}{mc\omega_p} \right) \frac{c}{\omega_p} = \frac{\delta n}{n_0}.$$

Finally we obtain

$$\nabla \cdot \frac{E_r}{\left(\frac{\omega_p}{c} E_{wb} \right)} \equiv \nabla \cdot E = \frac{\delta n}{n_0},$$

where $E = E_r/(\omega_p/c)E_{wb}$ is the electric field normalized by $(\omega_p/c)E_{wb}$. Since Maxwell equations tell us $\mathbf{E} = \beta_{ph}\mathbf{B}$ in electromagnetic waves, the magnetic fields are automatically normalized in the same way. At last, we have the corresponding normalized plasma momentum defined as $u = \gamma\beta$.

5.2.2 Charge and Current Densities

The charge and current densities on the grid are determined by weighting the charge of each particle between neighboring grid points. In em1da, the charge and current densities on the grid are obtained using the subtracted dipole scheme(SUD)[68] which performs with more accuracy and requires less storage and computation. This method follows: Assuming a particle with charge q_p and current $q_p v_p$ at position z_i, the charge and current are distributed to the nearest grids Z_j and its two neighbors, Z_{j+1} and Z_{j-1},

$$|z_i - Z_j| < \frac{\Delta}{2},$$

$$\begin{aligned}
\rho_j &= \frac{q_p}{\Delta}, \\
\mathbf{J}_j &= \frac{q_p\mathbf{v}_p}{\Delta}, \\
\rho_{j\pm1} &= \pm\frac{q_p}{\Delta}\left(\frac{z_i - Z_j}{2\Delta} \right) \\
\mathbf{J}_{j\pm1} &= \pm\frac{q_p\mathbf{v}_p}{\Delta}\left(\frac{z_i - Z_j}{2\Delta} \right).
\end{aligned}$$

where the subscript j denotes the grid j and Δ is the grid length taken to be unity. For $z_i = Z_j + \Delta/2$, the charge density at the neighboring grid will be $\rho_{j\pm1} = \pm q_p/4\Delta$.

5.2.3 Field Update

Once the charge density on the grid is given, we can solve the electrostatic potential and the associating electric field in k space from the Poisson equation,

$$
\begin{aligned}
\phi_k &= \frac{\mathrm{sm}(k)\rho_k}{k^2} \\
E_{zk} &= \frac{\mathrm{sm}(k)\rho_k}{k}
\end{aligned}
$$

where the source ρ_k is multiplied by a smoothing function $\mathrm{sm}(k)$,

$$
\mathrm{sm}(k) = \exp(-(\mathrm{ax} \cdot k)^{\mathrm{smp}}).
$$

The smoothing function is set up in order to attenuate the short wavelength components caused by the possible short range collisions between the single particle that represents many particles. Therefore the smoothing function defines the shape of the finite-size particle. Fig. 5.2 shows the smoothing function with different coefficients in ax and smp. The solid, dashed and dotted curves represent the function $\mathrm{sm}(k) = \exp(-k^3)$, $\exp(-(2k)^3)$, and $\exp(-(4k)^2)$ respectively. Once ϕ and E_{zk} are solved, the electric field in real space can be quickly computed from the inverse FFT of E_{zk}.

Next the Maxwell equations of transverse electromagnetic field $(\mathbf{E}_\perp, \mathbf{B}_\perp)$ in k-space are given as

$$
\begin{aligned}
\frac{\partial \mathbf{E}_\perp(\mathbf{k}, t)}{\partial t} &= -ic\mathbf{k} \times \mathbf{B}_\perp(\mathbf{k}, t) - \mathbf{J}_\perp(\mathbf{k}, t) \\
\frac{\partial \mathbf{B}_\perp(\mathbf{k}, t)}{\partial t} &= -ic\mathbf{k} \times \mathbf{E}_\perp(\mathbf{k}, t)
\end{aligned}
$$

We solve the above equations using the finite difference method with time central leapfrog scheme to stagger $\mathbf{B}_\perp$ at $n\Delta t$ coinciding with the velocity (see Sec. 5.2.4) and $\mathbf{E}_\perp$ at time level $(n-1)\Delta t$. The equations then become

$$
\begin{aligned}
\mathbf{E}_\perp^{n+1/2}(\mathbf{k}) &= \mathbf{E}_\perp^{n-1/2}(\mathbf{k}) + ic\Delta t\mathbf{k} \times \mathbf{B}_\perp^n(\mathbf{k}) - \mathrm{sm}(k) \cdot \mathbf{J}_\perp^n(\mathbf{k})\Delta t \\
\mathbf{B}_\perp^n(\mathbf{k}) &= \mathbf{B}_\perp^{n-1}(\mathbf{k}) - ic\Delta t\mathbf{k} \times \mathbf{E}_\perp^{n+1/2}(\mathbf{k})
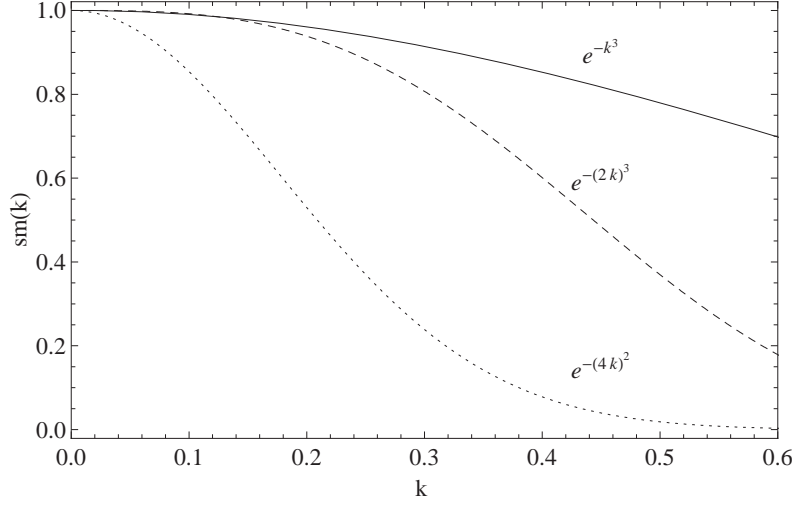\end{aligned} \tag{5.2}
$$

Figure 5.2: The smooth function with different parameters. The solid, dashed and dotted curves represent the function $\mathrm{sm}(k) = \exp(-k^3)$, $\exp(-(2k)^3)$, and $\exp(-(4k)^2)$ respectively.

after inserting the smoothing function, where n is the time series. $\mathbf{E}_\perp^{n+1/2}(\mathbf{k})$ is solved prior to $\mathbf{B}_\perp$ components. After advancing to $\mathbf{E}_\perp^{n+1/2}(\mathbf{k})$, $\mathbf{E}_\perp(\mathbf{k})$ is transformed back to real space and the outgoing boundary condition is applied by multiplying a masking function $f(Z_j)$ to this field. Fig. (5.3) shows the plot of the masking function used in the code. "ncdl" $(= 2^9)$ and "ncdr" $(= N_g - \mathrm{ncdl})$ defines the box edge where the transverse electric field starts to attenuate. The function $f(Z_j)$ is unity until Z_j reaching the edge and beyond that, $f(Z_j)$ will quickly drops to the half.

$\mathbf{B}_\perp^{n+1}(\mathbf{k})$ is updated after we apply the boundary condition to $\mathbf{E}_\perp^{n+1/2}(\mathbf{k})$. Since the Maxwell equations are solved in a discrete time, the stability of the electromagnetic wave determined by the choice of Δt should be concerned. To find the Courant-Friedrichs-Levy(CFL) condition for stability, we consider the vacuum case $(\mathbf{J}_\perp = 0)$ and substitute Eq. (5.2) with the assumptions that

$$\mathbf{E}_\perp(\mathbf{k}, t) = \mathbf{E}_0(\mathbf{k}) e^{-i\omega(n-1/2)\Delta t}$$
$$\mathbf{B}_\perp(\mathbf{k}, t) = \mathbf{B}_0(\mathbf{k}) e^{-i\omega n \Delta t}.$$

It gives

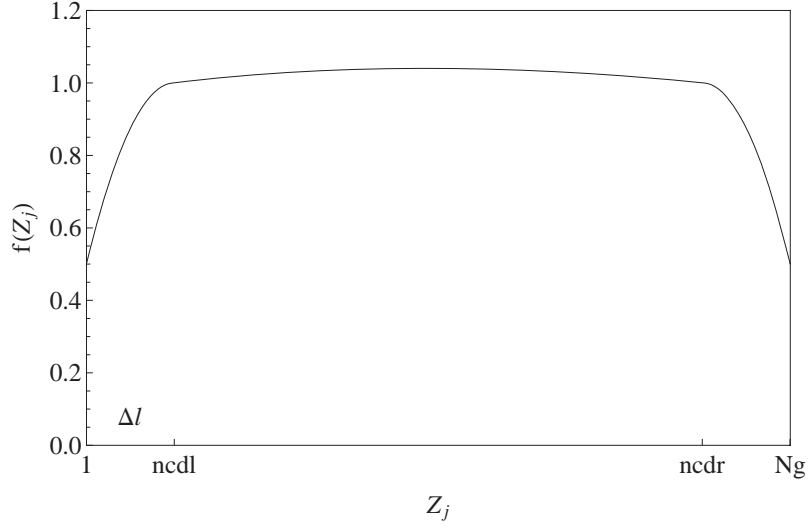$$c^2 k^2 = \frac{\sin^2(\omega \Delta/2)}{(\Delta t/2)^2} \tag{5.3}$$

Figure 5.3: The masking function with ncdl = 2^9 and ncdr= $N_g -$ ncdl.

which approaches the correct behavior that $c^2 k^2 = \omega^2$ as $\Delta t \to 0$. For finite Δt, there are real solutions for ω only if

$$ck(\Delta t/2) < 1. \tag{5.4}$$

If the inequality is not satisfied then the solutions of frequencies are complex and the system is unstable. This condition Eq. (5.4) implies that the time step Δt is limited by the largest k-mode.

5.2.4 Particle Update

In calculating the integration of particle equation of motion, we construct a leapfrog scheme with the particle positions defined at $(n-1/2)\Delta t$ and velocities at $n\Delta t$. So the finite-difference form for the Lorentz-Newtonian equations in Eq. (5.1a) and (5.1b) becomes

$$
\begin{aligned}
z_i^{n+1/2} &= z_i^{n-1/2} + v_{zi}^n \Delta t, \\
\mathbf{v}_i^{n+1} &= \mathbf{v}^n + \frac{q_i \Delta t}{m_i} \left[\mathbf{E}_i^{n+1/2} + \frac{(\mathbf{v}_i^{n+1} + \mathbf{v}_i^n) \times \mathbf{B}_i^{n+1/2}}{2c} \right],
\end{aligned} \tag{5.5}
$$

where $\mathbf{B}_i^{n+1/2} = (\mathbf{B}_i^n + \mathbf{B}_i^{n+1})/2$. The fields are inversely interpolated from spatial grids to the particle locations with the same weighting,

$$\mathbf{E}(z_i) = \mathbf{E}_j + \frac{z_i - Z_j}{2}\mathbf{E}_{j+1} - \frac{z_i - Z_j}{2}\mathbf{E}_j$$
$$\mathbf{B}(z_i) = \mathbf{B}_j + \frac{z_i - Z_j}{2}\mathbf{B}_{j+1} - \frac{z_i - Z_j}{2}\mathbf{B}_j.$$

To effectively solve these equation, we perform a time-splitting method[69] and define

$$\mathbf{v}_i^- = \mathbf{v}_i^n + \frac{q_i \Delta t}{2m_i}\mathbf{E}_i^{n+1/2}, \tag{5.6}$$

$$\mathbf{v}_i^+ = \mathbf{v}_i^{n+1} - \frac{q_i \Delta t}{2m_i}\mathbf{E}_i^{n+1/2} \tag{5.7}$$

to be substituted into Eq. (5.5). It gives

$$\mathbf{v}_i^+ - \mathbf{v}_i^- = \frac{q_i \Delta t}{2m_i c}(\mathbf{v}_i^+ + \mathbf{v}_i^-) \times \mathbf{B}_i^{n+1/2},$$

which represents a rotation of momentum associating with $\mathbf{B}$. Thus by performing this method, the particle is first half-accelerated from $\mathbf{v}^n$ to $\mathbf{v}^-$ with Eq. (5.6) and then rotate according to Eq. (5.8). The last half acceleration is added in the following to obtain $\mathbf{v}_i^{n+1}$ with Eq. (5.6).

5.2.5 Computation Cycle

In summarizing the steps of the code, we list the computation cycle which involved in advancing the electromagnetic fields and particles for one time step[67],

Initialization: $z_i^{n-1/2}, \mathbf{v}_i^n, \mathbf{E}_\perp^{n-1/2}$ and $\mathbf{B}_\perp^n$

Step 1: Advance $z_i^{n-1/2}$ to z_i^n and accumulate the current $\mathbf{J}^n$ on the grid j

Step 2: Advance z_i^n to $z_i^{n+1/2}$ and accumulate the charge $\rho^{n+1/2}$ on the grid j

Step 3: Transform $(\rho^{n+1/2}, \mathbf{J}^n)$ to k-space giving $(\rho^{n+1/2}(k), \mathbf{J}^n(k))$

Step 4: Solve the $E_z^{n+1/2}(k)$ using $\rho^{n+1/2}(k)$

Step 5: Advance $\mathbf{E}_\perp^{n-1/2}(k)$ to $\mathbf{E}_\perp^{n+1/2}(k)$ by $\mathbf{B}_\perp^n(k)$ and $\mathbf{J}^n(k)$

Step 6: Advance $\mathbf{B}_\perp^n(k)$ to $\mathbf{B}_\perp^{n+1}(k)$ by $\mathbf{E}_\perp^{n+1/2}(k)$

Step 7: Transform $(\mathbf{E}_\perp^{n+1/2}(k), \mathbf{B}_\perp^{n+1}(k))$ back to real space.

Step 8: Interpolate the field from grids to particles.

Step 9: Advance the particle $\mathbf{v}_i^n$ to $\mathbf{v}_i^{n+1}$ using these fields.

5.3 The MPWA Simulation

To study the MPWA mechanism, we set up a whistler Gaussian wavepacket propagating parallel to the external magnetic field in plasma, which is a medium wave and considered to be self-generated in the magnetized plasma.

5.3.1 Initialization

The geometry of the simulation is shown in Fig. 5.4. We deal with the plasma dynamics in the phase space (z, p_x, p_y, p_z) with the external magnetic field imposed along the z direction. The basic parameter inputs are these in the followings. The total number of grids as well as the length of simulation box in the z-direction is $L_z = 2^{14}\Delta = 546c/\omega_p$ where Δ is the grid length taken to be unity. The particles are uniformly distributed with average number per grid as 10. The particle velocities including thermal and drift are initially zero. Thus the plasma temperature defined by particle thermal motion is zero for both species. The mass ratio of ion to electron is 2000 and the skin depth is $c/\omega_p = 30\Delta$, which gives a normalization factor $1/30E_{wb}$ to the electric and magnetic fields according to sec. 5.2.1. The smoothing function is set $\exp(-(2k)^3)$ with ax=2 and smp=3.

Whistler Pulses

To generate the whistler Gaussian wavepacket, it is essential to set a high ω_c/ω_p ratio in order to make the dispersion relation more linear over a larger wavenumber range. Consequently, the pulse can travel a long distance with minor dispersion. During the initialization stage, the whistler wavepacket was artificially given

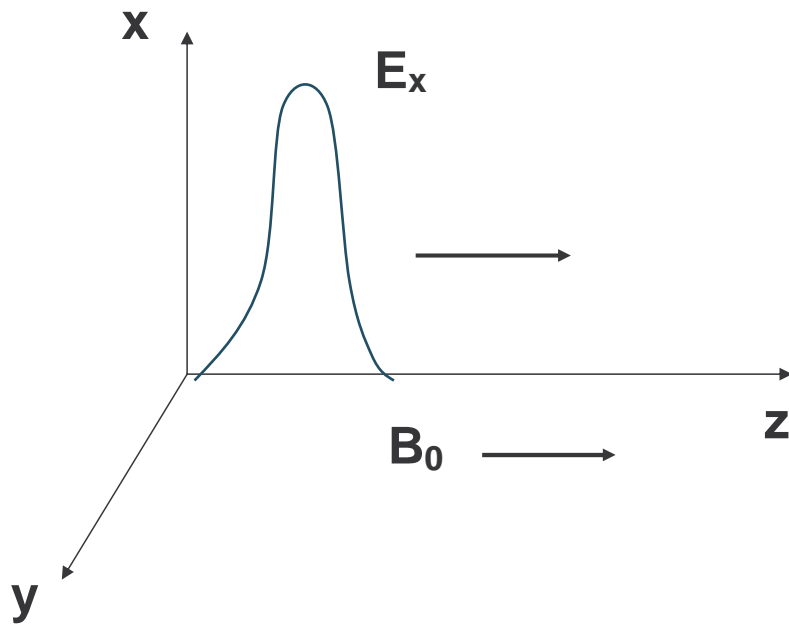$$E_x(Z_j) = E_\perp(nt) \cdot \beta_{ph} \exp\left(-\frac{Z_j - Z_{pos}}{2\sigma^2}\right) \cos(k(Z_j - Z_{pos}))$$

Figure 5.4: The sketch of the geometry in simulation, with an external magnetic field B_0 imposed along the z direction. The whistler pulse is set to propagate parallel to B_0.

by the program ignoring the plasma reaction. The phase velocity $\beta_{ph} = \omega/ck$ was calculated from the dispersion relation,

$$\omega^2 = k^2 c^2 + \frac{\omega_p^2}{1 - \omega_c/\omega} + \frac{\omega_{ip}^2}{1 + \omega_{ic}/\omega}. \qquad (5.8)$$

The amplitude of pulse is linearly increased to avoid the possible spurious effect

$$E_\perp(nt) = \frac{E_{\perp 0}}{T_{\text{ramp}}} nt, \quad nt \leq T_{\text{ramp}} \qquad (5.9)$$

until reaching the maximum amplitude $E_{\perp 0}$ at $nt = T_{\text{ramp}}$. The pulse then starts to self-consistently evolve with time according to Maxwell equations.

In our simulation, two cases with $\omega_c/\omega_p = 6$ (case a) and 12 (case b) are performed. For the two cases, the time step is set to $\Delta t = 0.1\omega_p^{-1}$ for case a and $\Delta t = 0.05\omega_p^{-1}$ for case b to resolve the different ω_c. Considering the plasma wavelength $\lambda_p \sim 2\pi c/\omega_p \sim 188.5\Delta$, we set the wavenumber $k = 2\pi/60\Delta$, $2\pi/40\Delta$ with the same Gaussian width $\sigma = 80\Delta/\sqrt{2}$ for case a and b respectively. They give $\omega/\omega_p = 2.98$, $v_{ph}/c = 0.95$ for case a and $\omega/\omega_p = 4.64$, $v_{ph}/c = 0.99$ for case b from the dispersion relation. The pulse is initialized at $Z_0 = 500\Delta = 16.66c/\omega_p$ with $E_{\perp 0} = 8.05$ $(0.27E_{wb})$ and $T_{\text{ramp}} = 100\omega_p^{-1}$ for case a, while $E_{\perp 0} = 20(0.67E_{wb})$ and $T_{\text{ramp}} = 200\omega_p^{-1}$ for case b. That implies the associated strength parameters $a_0 \equiv E_{\perp 0}/mc\omega$ are 0.09 and 0.14 respectively. Clearly the two cases are both in the linear regime. Thus the accelerating gradient G can be predicted as 0.17 $(0.0057eE_{wb})$ from Eq. (3.10) for both cases (or more accurate results, see [43]). Figure 5.5(a) and 5.5(b) are the whistler pulses in case a and b plotted in k space imposed with their associated phase velocities to ensure all modes having similar phase velocities.

5.3.2 Results

Plasma Wakefield

In our simulation, the total simulation time is set $500\omega_p^{-1}$. After the pulse was released from the initialization (at $nt = T_{\text{ramp}}$), the whistler wavepackets self-consistently evolve during the time. Evidently, we can see the plasma wakefield was excited behind the driving pulses in both cases even in the initialization stage. Figure 5.6(a) and 5.6(b) are the snapshots of the driving pulse and plasma wakefield at $\Delta t = 100\omega_p^{-1}$ after the pulse released. We can see that
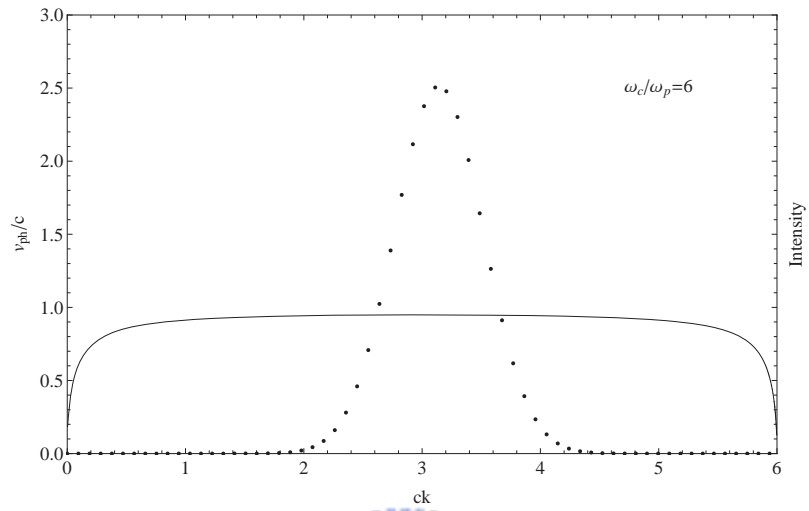
(a) case a
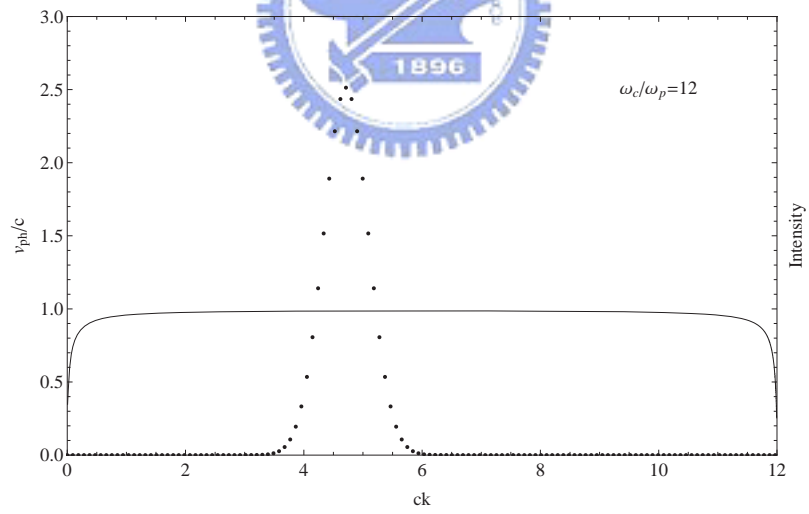
(b) case b

Figure 5.5: The intensity plot of the driving pulses in k space (in arbitrary unit) imposed with their associated phase velocities in case a and b.

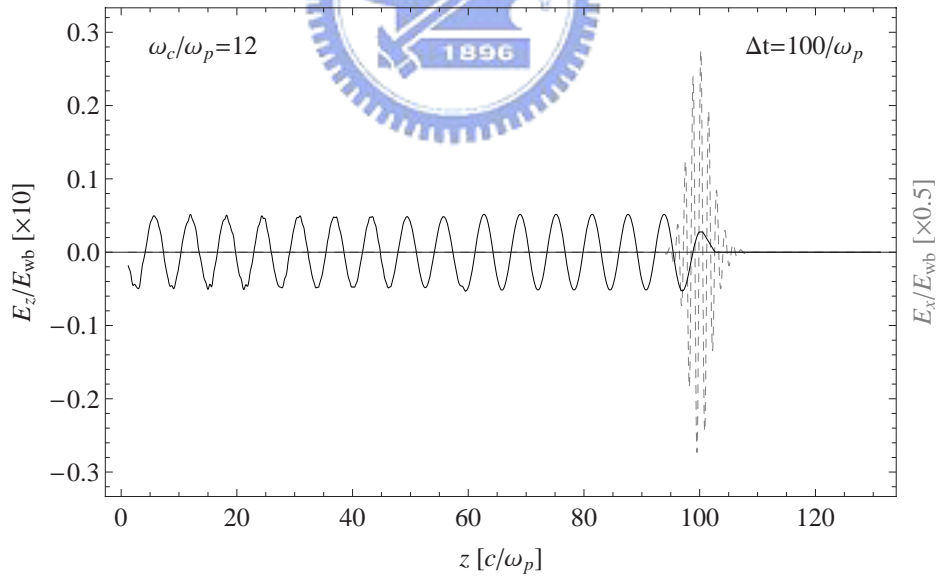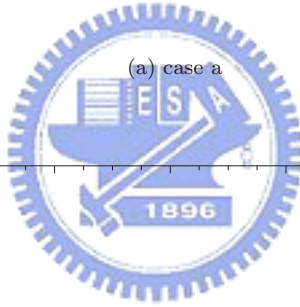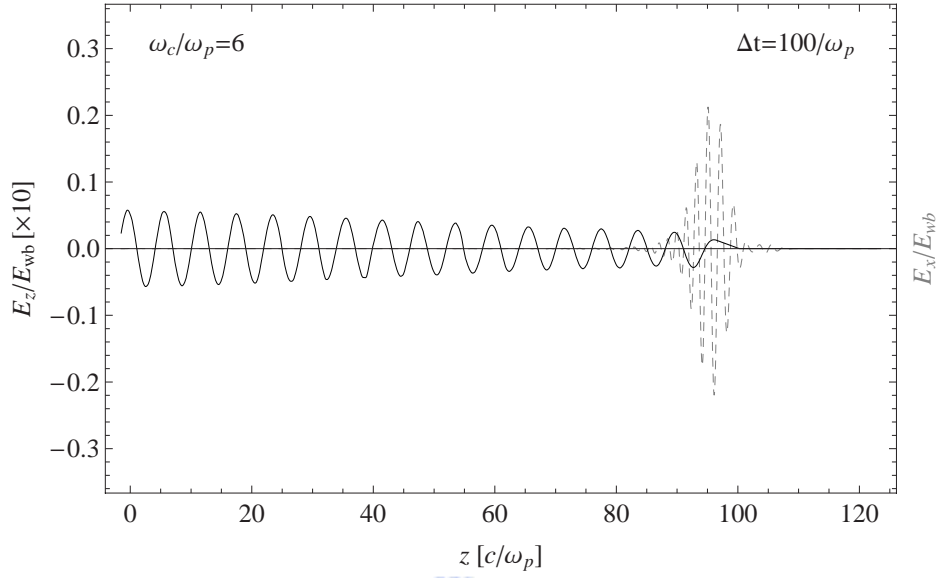Figure 5.6: The snapshot of the whistler pulse (gray dashed) and the excited plasma wakefield (solid) in case a and b at $\Delta t = 100\omega_p^{-1}$ after pulse released.

the maximum amplitude of plasma wakefield in both cases is around $0.0057E_{wb}$ and the plasma wavelength is $\sim 2\pi c/\omega_p$, agreed with the theoretical prediction. However in case a, because the dispersion relation is not perfectly linear, the pulse disperses during the propagation. As a result, the amplitude of plasma wakefield would also decrease due to the pulse dispersion.

Figure 5.7(a) shows that the driving pulse become severely spread at a late time $\Delta t = 300\omega_p^{-1}$. The plasma wakefield is generated with a much smaller amplitude but remains coherent. However this situation can be greatly improved with a higher ω_c/ω_p ratio as case b in Fig. 5.7(b). We see that the driving pulse is barely dispersed even running after a long distance and the corresponding wakefield amplitude remains constant.

Dispersion Relation

Next we show the intensity contours of the driving pulses in the two cases in $\omega - k$ space. Here each time step was set to $\omega\Delta t = 0.1$ for both cases. Owing to the restriction of storage memory, we shrink the simulation box size from $L_z = 2^{14}\Delta$ to $L_z = 2^{12}\Delta$. The E_x component of the driving pulses in k space was sampled every time step after the pulse released. The number of sampling is $N = 500$ and therefore the sampling time is $N\Delta t = 50\omega_p^{-1}$. So that we have $E_x(t_n, k_l)$ recorded in the time series t_n, where $k_l = l(2\pi/L)$ and $t_n = n\Delta t$.

$E_x(\omega_m, k_l)$ is obtained from the Fourier transformation of $E_x(t_n, k_l)$,

$$E_x(k_l, \omega_m) = \sum_{n=0}^{N-1} E_x(k_l, t_n) \exp(-i\omega_m t_n),$$

where $\omega_m = m2\pi/(50\omega_p^{-1})$. The result is illustrated in Fig. 5.8 where the two contours represent the cases for $\omega_c/\omega_p = 6, 12$ and are superimposed with the theoretical curves for the whistler wave dispersion relations deduced from Eq. (5.8). The dotted line shows the light curve. It is obvious to see the contours agree well with the two theoretical curves. we confirm that our driving pulses were indeed whistler waves.

Energy Conservation

Without the energy supplying and dissipating process, the total energy of the system should be conserved. It is possible to check the stability of the system
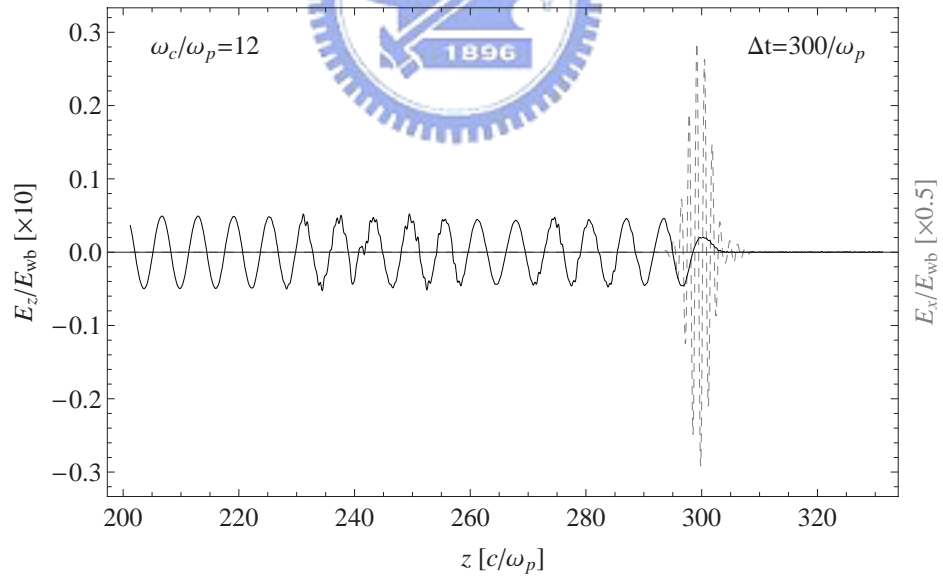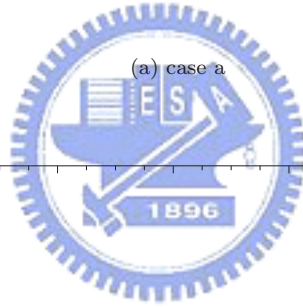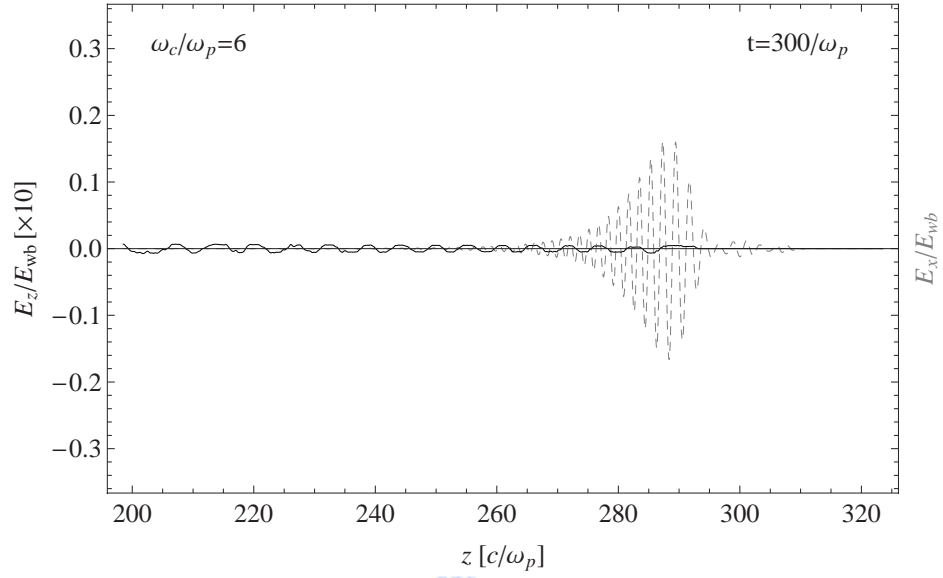
(a) case a

(b) case b

Figure 5.7: The snapshot of the whistler pulse (gray dashed) and the excited plasma wakefield (solid) in case a and b at $\Delta t = 300\omega_p^{-1}$ after pulse released.
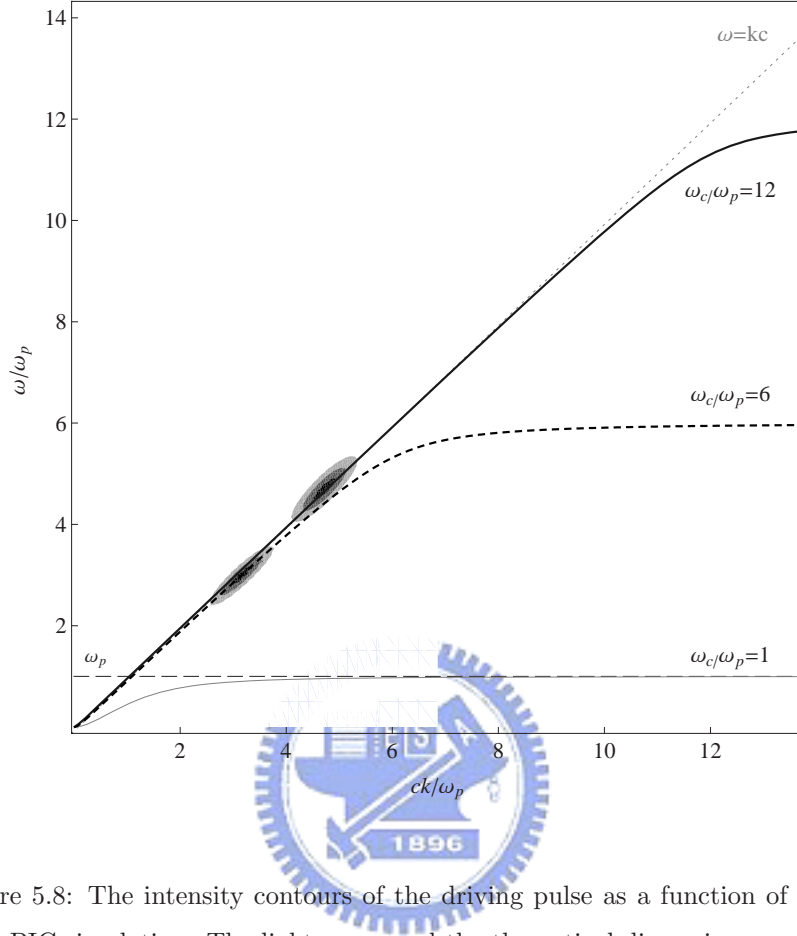
Figure 5.8: The intensity contours of the driving pulse as a function of (ω, k) from PIC simulation. The light curve and the theoretical dispersion curves for the whistler wave with $\omega_c/\omega_p = 1, 6$ and 12 are superimposed.

by investigating the conservation of total energy. Hence during the simulation, the kinetic energy of particles, electrostatic field energy and the electromagnetic field are calculated at every time step and stored. The total energy is the sum of the particle kinetic energies and field energies. Figure 5.9 shows the plot of the total energy versus the simulation time in the case b with the vertical axes in arbitrary unit. We can see that, at beginning, the total energy rises up due to the pulse initialization. After the pulse was released at $T_{ramp} = 200\omega_p^{-1}$, the total energy maintains a constant value.
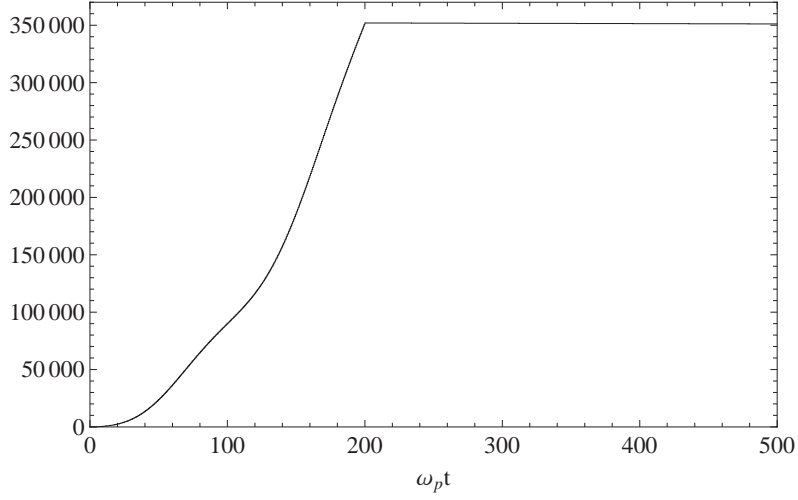
Figure 5.9: The total energy (in arbitrary unit) versus simulation time in case b.

Accelerating Gradient

Finally, we validate the functional dependence of the acceleration gradient given by the solution of Eq. (4.21). In this simulation, the ω_c/ω_p ratio is set to be 12. The wavepackets are initialized with a fixed wavenumber $k = 2\pi/60\Delta$ so that the frequency of the pulse is solved as $\omega/\omega_p = 3.1$. The pulse electric field $E_{\perp 0}$ is varied from 10 to 80 (in unit of $1/30E_{wb}$) and the strength parameter a_0 varies accordingly. We plot the acceleration gradient G versus the varying a_0, as shown in Fig. 5.10. The points are the simulation data and the solid curve is the theoretical curve obtained by solving Eq. (4.21),

$$\frac{\partial^2 \phi}{\partial \zeta^2} = \frac{k_p^2}{2} \left[\left(\frac{a^2}{(1 - \frac{\omega_c}{\omega(1+\phi)})^2} + 1 \right) \frac{1}{(1+\phi)^2} - 1 \right].$$

In addition the dashed curve is the extrapolation of the non-relativistic result, Eq. (4.10),

$$G = \frac{a_0^2}{(1 - \frac{\omega_c}{\omega})^2} \chi e E_{wb},$$

, which is valid only in the $a_0 \ll \omega_c/\omega - 1 \, (\sim 3)$ limit. We see that the simulation data points agree well with the theoretical curve of relativistic MPWA equation.

63
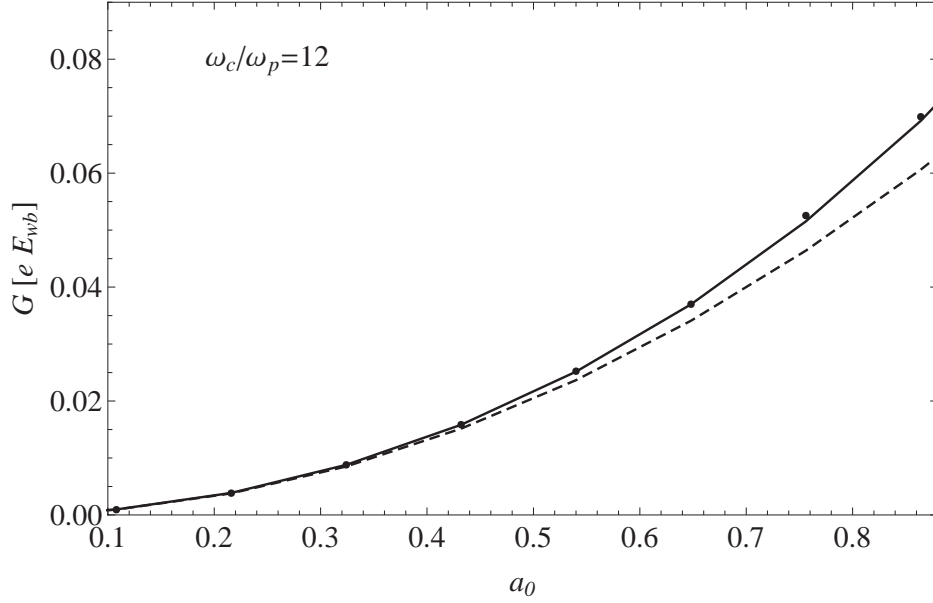
Figure 5.10: The plot of accelerating gradient G versus a_0. The simulation data points agree well with the solid curve obtained by solving Eq. (4.21). The dashed curve is the extrapolation of the non-relativistic theoretical result, Eq. (4.10).

5.4 Summary

To summarize the study of plasma simulation, we have successfully demonstrated a whistler gaussian pulse that can be self-generated in the magnetized plasma and travels a sufficient distance. The corresponding plasma wakefield is excited behind the pulse with amplitude in agreement with the theoretical prediction. We also confirm the relativistic MPWA equation Eq. (4.21) via the self-consistent plasma simulation.

Chapter 6

Applications to UHECR

Now, we have completely established the MPWA theory via analytical and particle simulation approaches. This theory does not rely on any outer source for plasma wakefield excitations and involves a linear acceleration process in the advantage of minimizing the energy loss due to particle bending. Now we are ready to apply this theory to explain the production of UHECRs. By looking at the cosmic ray spectrum, we notice that there are two crucial facts for an acceleration model: the differential power-law spectrum $dN/dE \propto E^{-3}$ and the high efficiency in energy gain. The conventional model diffusive shock acceleration(DSA) gives the injection power index ~ -2 for non-relativistic and $\sim -(2.2 - 2.3)$ [21, 22] for relativistic shocks. We will show that, the MPWA mechanism can also produce a power law spectrum through the stochastic processes with index -2 in an idea case and have a high accelerating gradient for particles to gain energy up to 10^{21} eV.

6.1   Power-Law Spectrum

From our knowledge of a terrestrial plasma accelerator, the wakefields are coherently excited by the driving beam and the accelerating particle rides on the same wave crest over a macroscopic distance. Since the speed of the driving beam as well as the wakefield phase velocity can not exceed the speed of light, the accelerating particle will eventually escape the acceleration phase (the so-called phase slippage) and the maximum acceleration distance is then determined. However

for the astrophysical settings, the driving pulses such as the magneto-shocks, are not so organized. Instead, they will be produced randomly by the progenitor and a test particle would then face random encounters of accelerating and decelerating phases of the induced plasma wakefield. Meanwhile, some degradations such as the dispersion of the driving magneto-shocks or phase slippage between the test particle and the wakefield, would eventually throw the test particle out of the acceleration phase into the deceleration phase, and vise versa. Thus finally the test particle gets accelerated and decelerated stochastically during the particle-wakefield interactions. The particle energy distribution function $f(\epsilon, t)$ is then governed by the Chapman-Komogorov equation[70, 71]

$$\frac{\partial}{\partial t} f(\epsilon) = \int_{-\infty}^{\infty} d(\Delta\epsilon) W(\epsilon - \Delta\epsilon) f(\epsilon - \Delta\epsilon, t) - \int_{-\infty}^{\infty} d(\Delta\epsilon) W(\epsilon) f(\epsilon, t)$$
$$- \nu(\epsilon) f(\epsilon) \tag{6.1}$$

, where $W(\epsilon, \Delta)$ is the transition rate of a particle from energy ϵ to $\epsilon \pm \Delta\epsilon$. The first term at the right hand side is the probability rate of a particle "sinking" into energy ϵ from an initial energy $\epsilon - \Delta\epsilon$ and the second term is that of particle "leaking" out of energy ϵ. The last term proportional to $f(\epsilon, t)$ governs all possible dissipations, such as collision or radiation, or both. In an ideal condition, we may ignore the dissipation term in Eq. (6.1) and have a purely random acceleration-deceleration particle-wakefield interaction equation. If we assume that the energy gain per phase encounter $\Delta\epsilon$ is much less then the final energy, i.e., $\Delta\epsilon \ll \epsilon$, we can expand the $W(\epsilon - \Delta\epsilon) f(\epsilon - \Delta\epsilon, t)$ to the second order, that is,

$$
\begin{aligned}
&W(\epsilon - \Delta\epsilon, \Delta\epsilon) f(\epsilon - \Delta\epsilon, t) \\
=~&\left(W(\epsilon, \Delta\epsilon) - \frac{\partial}{\partial\epsilon} W(\epsilon, \Delta\epsilon) \Delta\epsilon + \frac{\partial^2}{\partial\epsilon^2} W(\epsilon, \Delta\epsilon) \Delta\epsilon^2 + \dots \right) \\
&\times \left(f(\epsilon, t) - \frac{\partial}{\partial\epsilon} f(\epsilon, t) \Delta\epsilon + \frac{\partial^2}{\partial\epsilon^2} f(\epsilon, t) \Delta\epsilon^2 + \dots \right) \\
=~&W(\epsilon, \Delta\epsilon) f(\epsilon, t) - \frac{\partial}{\partial\epsilon} W(\epsilon, \Delta\epsilon) f(\epsilon, t) \Delta\epsilon + \frac{\partial^2}{\partial\epsilon^2} W(\epsilon, \Delta\epsilon) f(\epsilon, t) \frac{\Delta\epsilon^2}{2}
\end{aligned}
\tag{6.2}
$$

Inserting Eq. (6.2) to Eq. (6.1), we can reduce the Chapman-Kolmogorov equation to the Fokker-Planck equation

$$\frac{\partial}{\partial t}f(\epsilon) = \frac{\partial}{\partial \epsilon}\int_{-\infty}^{\infty}d(\Delta\epsilon)\Delta\epsilon W(\epsilon,\Delta\epsilon)f(\epsilon,t)$$
$$- \frac{\partial^2}{\partial\epsilon^2}\int_{-\infty}^{\infty}d(\Delta\epsilon)\frac{\Delta\epsilon^2}{2}W(\epsilon,\Delta\epsilon)f(\epsilon,t) \tag{6.3}$$

In comparison with the Fokker-Planck equation describing the particle Brownian motion in the fluid, the first term $\Delta\epsilon W(\epsilon,\Delta\epsilon)$ of Eq. (6.3) may correspond to the the drift term and the second term is the diffusion term.

Now we can make an assumption of the transition rate $W(\epsilon,\Delta\epsilon)$ for a purely stochastic process under the following properties of the particle wakefield interaction: 1) in the acceleration and deceleration processes, the probability of gaining and losing energy should be equal; 2) moreover, unlike the shock diffusive acceleration in which the energy gain is proportional to the particle recent energy, the wakefield amplitude is independent of particle energy, that is, the chance of gaining amount of energy, $\Delta\epsilon$, is independent of ϵ; 3) and finally, under a pure stochastic white noise, the chance of gaining or losing any energy amount $\Delta\epsilon$ is the same. Based on these arguments, we have the properties of the $W(\epsilon,\Delta\epsilon)$:

a) W is an even function,

b) W is independent of ϵ,

c) W is independent of $\Delta\epsilon$.

It is then reasonable to deduce that[71]

$$W(\epsilon,\Delta\epsilon) = \frac{1}{2c\tau^2 G}, \tag{6.4}$$

where τ is the typical interaction time between the test particle and random plasma wakefield and G is the maximum acceleration gradient. The stationary solution for Eq. (6.3) is easily obtained by putting the temporal term $\partial f/\partial t = 0$. Since W is an even function, the first term on the right hand side of Eq. (6.3) should vanish because it has only one power of $\Delta\epsilon$. Sequently the remaining equation becomes

$$\frac{\partial^2}{\partial\epsilon^2}\int_{-\infty}^{\infty}d(\Delta\epsilon)\frac{\Delta\epsilon^2}{2}W(\epsilon,\Delta\epsilon)f(\epsilon) = 0. \tag{6.5}$$

To ensure the positivity of particle energies before and after each encounter, the integration limits are reduced from $(-\infty, \infty)$ to $[-\epsilon, \epsilon]$ and Eq. (6.5) becomes

$$\frac{\partial^2}{\partial \epsilon^2} \int_{-\epsilon}^{\epsilon} d(\Delta\epsilon) \frac{\Delta\epsilon^2}{2} W(\epsilon, \Delta\epsilon) f(\epsilon, t) = 0 \qquad (6.6)$$

Substituting Eq. (6.4) into the above equation, we can solve the equation and arrive at the power-law distribution function,

$$f(\epsilon) = \frac{\epsilon_0}{\epsilon^2}, \qquad (6.7)$$

where ϵ_0 is taken to be the initial energy of the proton. The power law index is exactly -2 in the ideal case caused by the stochastic process[71]. However the actual observed spectrum would be expected to be degraded somehow due to the various inevitable energy loss mechanisms. The resulting spectrum is as the form, $f(\epsilon) \propto 1/\epsilon^{-(2+\beta)}$ with $\beta > 0$. Phenomenologically, the allowed range for β can be determined by performing fittings to the measured UHECR spectrum[72].

6.2 Possible Sources for UHECRs

On the cosmic ray spectrum, there are two kinks indicating the changes of the power law indices. The one at $10^1 8$ eV (the "ankle") is commonly believed caused by the source transition from galactic to extragalactic. Based on that, the UHECR origin is conventionally considered to be extragalactic. However the actual source of UHECRs so far is not yet understood. Relying on the Fermi mechanism, A. M. Hillas in 1984 proposed his famous plot to identify the possible sources capable of accelerating particle to 10^{20-21} eV[73]. If a particle with charge Ze gains energy gradually from many irregular collisions with magnetic turbulence, it will eventually escape the acceleration site when its Larmor radius exceeds the accelerator of size L. As a result the maximum energy of the particle is constrained by

$$E_{max} \sim ZBL. \qquad (6.8)$$

Figure 6.1 shows the astrophysical objects plotted with their magnetic field strength and sizes.
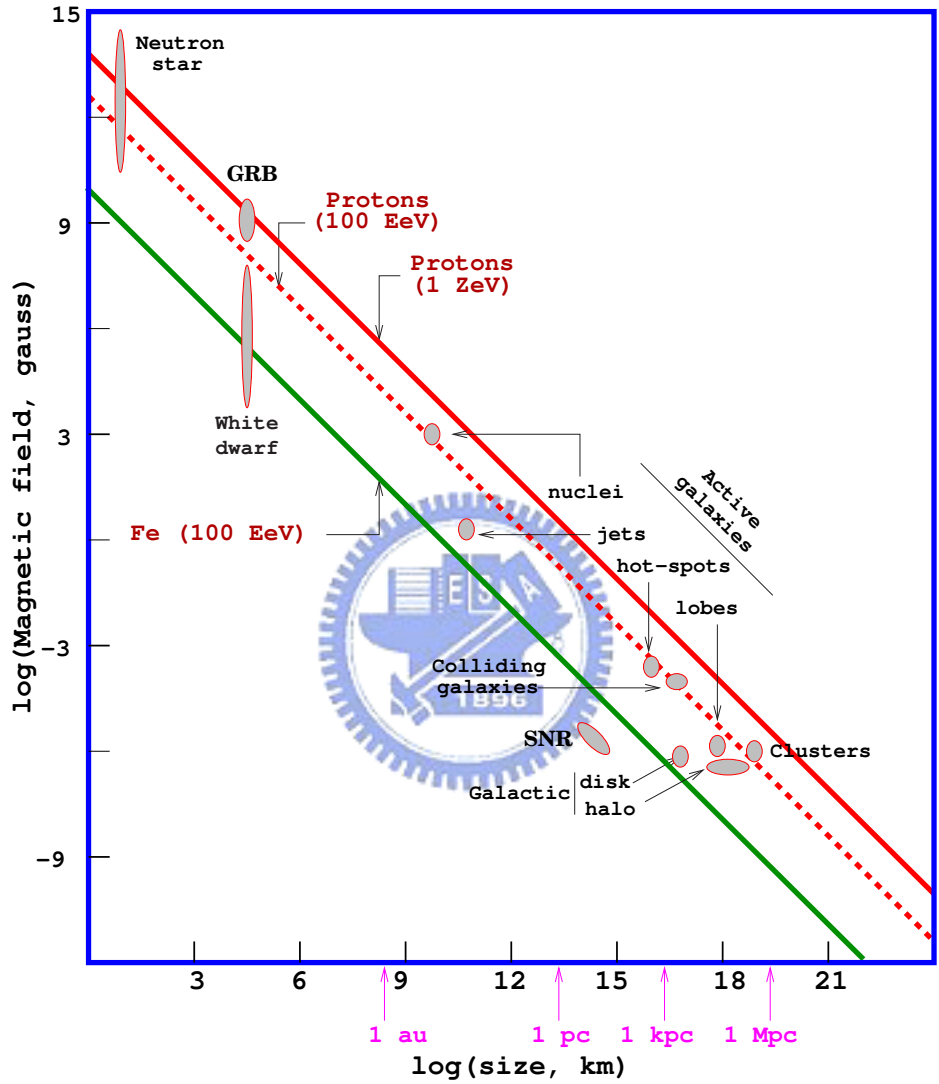
Figure 6.1: The famous Hillas plot, showing the astrophysical objects with their magnetic field strength and sizes. The solid lines representing $E_{max} \sim ZBL$ and $E_{\max} = ZBL\Gamma$ are also shown.

The green line is for the iron nuclei with an energy $10^{20}eV$ and the solid and dotted lines in red are for protons energies of with 10^{21} eV and 10^{20} eV respectively. It is shown that several objects are possible candidates for UHECR. However regarding the parallel magnetic field background, our MPWA mechanism is not subject to the concept. Nevertheless it still provide a good thought on the candidate sources of UHECRs.

Since the GRB and AGN are two most powerful objects in the universe, they have been discussed in several literature as the candidate sources for UHECR (for GRB [74, 75]; for AGN[76, 77]). With such high energies, the UHECRs are expected to deviate only slightly from their original trajectories by the extragalactic magnetic fields. Consequently the anisotropy of cosmic ray direction corresponding to the astrophysical objects can be a clue of the possible sources. So far the observations show that the observed direction of most UHECRs are uniformly distributed. The Pierre Auger Collaboration recently reported a possible correlation of UHECR with the nearby extragalactic AGN[78, 79]. This finding however has not been confirmed by HiRes[80]. Hence the source for UHECR remains an open issue.Here we invoke AGN as the site for the MPWA production of UHECR to illustrate the effectiveness of our mechanism.

6.3   Application to AGNs

An AGN is powered by the gravitational energy released from the accretion disk formed by its central super massive black hole(SBH) and typically releases its energy through relativistic jets that extend a distance far greater than the size of its core with negligible diverging angle. The typical Lorentz factor for the relativistic jet is ~ 10. Since the constitution of jets is still debated, we assume that the jets are consist of electrons and protons, with the total length from few kpc to Mpc. Based on that, we can reasonably simplify the geometry by modeling the jet as a cylinder(see Fig. 6.2) which contains a constant plasma density and magnetic field strength over a large distance. The accelerating gradient is then estimated with those characteristic parameters evaluated near the AGN central engine.

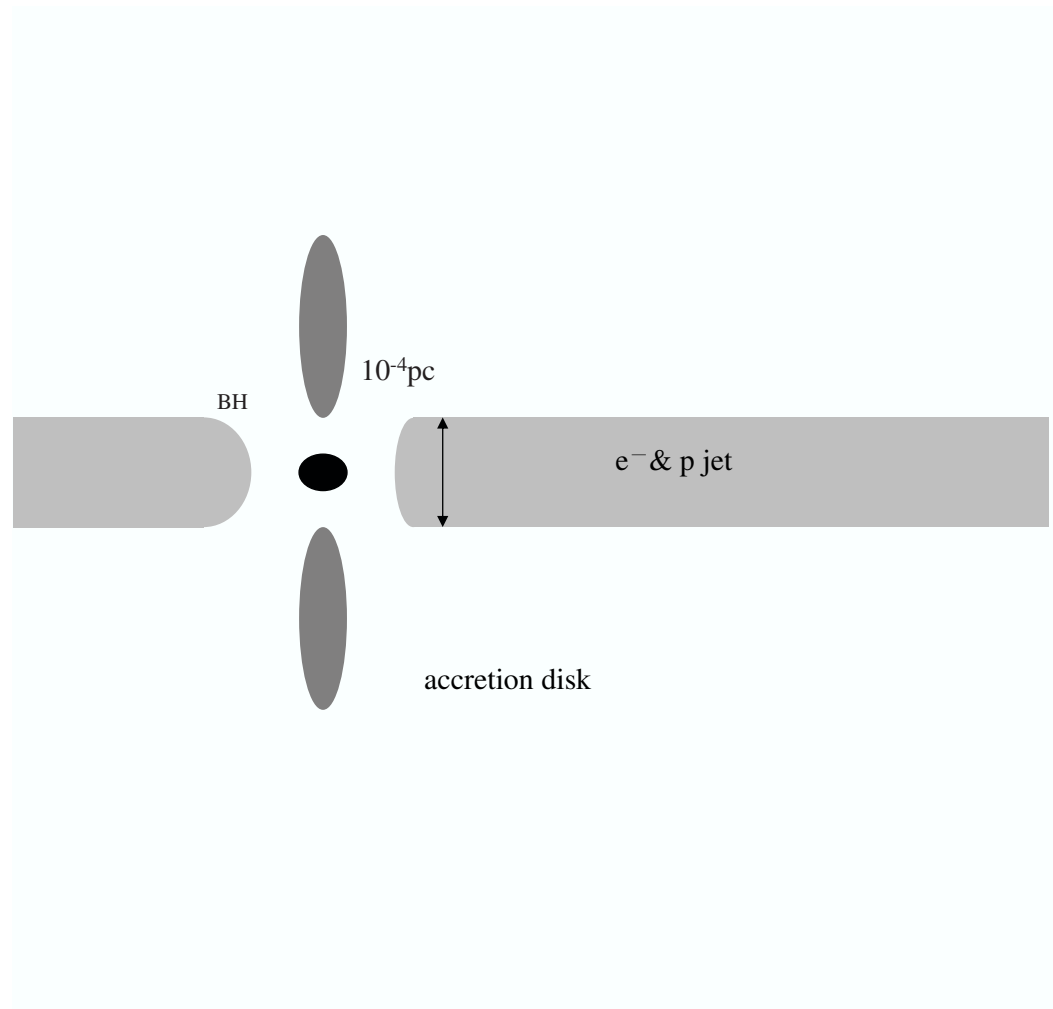The maximum luminosity an AGN can achieve is restricted by the Eddington

Figure 6.2: The simplified $e^- - p$ jet geometry with ignoring the divergence angle. The plasma density and background magnetic field strength are considered as constant.

limit at which the outward radiation pressure is equal to the inward gravitational force.

$$
\begin{aligned}
L_{Edd} &= \frac{4\pi GMm_pc}{\sigma_T} \\
&\cong 1.3 \times 10^{31} \left(\frac{M}{M_\odot}\right) W = 3.3 \times 10^4 \left(\frac{M}{M_\odot}\right) L_\odot,
\end{aligned}
$$

where $\sigma_T = 8\pi/2(\alpha\hbar/mc)$ is the Thompson scattering cross section for electron. With a central SBH mass $\sim 10^8 M_\odot$, the maximum luminosity of AGN is $\sim 10^{46} erg/s$ and the size of jet is roughly the size of the accretion disk $\sim 3R_s \sim 10^{-4}$pc, where R_s is the Schwarzschild Radius

$$
R_s = \frac{2GM}{c^2}. \tag{6.9}
$$

For an AGN jet having the maximum luminosity implies the plasma density

$$
n \simeq 10^{10} \left(\frac{L}{L_E}\right) \left(\frac{V_{\text{freefall}}}{V_{\text{infall}}}\right) M_8 \text{cm}^{-3} \sim 10^{10} \text{cm}^{-3} \tag{6.10}
$$

and the magnetic field,

$$
B \simeq 10^4 \left(\frac{L}{L_E}\right)^{1/2} \left(\frac{V_{\text{freefall}}}{V_{\text{infall}}}\right)^{1/2} M_8^{-1/2} G \sim 10^4 G \tag{6.11}
$$

near the core with M_8 defining as $M/(10^8 M_\odot)$, V_{freefall}, the free fall (or Kaplerian) speed, being of the order the inward drift speed V_{infall}[81]. The corresponding plasma and electron cyclotron frequencies are obtained, $\omega_p \sim 5.6 \times 10^8 \sim 10^9$ rad/s and $\omega_c \sim 10^{11}$rad/s and the ratio of ω_c/ω_p is about 10^2. The temperature is estimated as the black body temperature in the core as

$$
T \simeq 3 \times 10^5 \left(\frac{L}{L_E}\right)^{1/4} M_8^{-1/4} \sim 10^5 \text{K}. \tag{6.12}
$$

and the Debye length is given by

$$
\lambda_D = \sqrt{\frac{T}{4\pi ne^2}} \simeq 10^{-3} \text{m} \tag{6.13}
$$

which is much smaller compared to the plasma wavelength $\lambda_p = 2\pi c/\omega_p \sim 3$ m. Thus we ensure the validity of plasma collective effect in AGN jets.

With these characteristic parameters, it is possible to estimate the accelerating gradient of MPWA produced in jets. First we calculate the average strength parameter $a_0 = eE_0/m_ec\omega$ from the following relation

$$
a_0^2 = 4\pi \frac{e^2}{m_e^2c^2\omega^2} \left(\frac{E_0^2}{4\pi}\right) = 4\pi \frac{e^2}{m_e^2c^2\omega^2} \eta u_{AGN} \tag{6.14}
$$

where u_{AGN} is the total energy density in the jets and η the energy fraction imparted into the magnetowave modes. The energy density u_{AGN} can be easily computed from the total luminosity,

$$u_{AGN} = \frac{L \cdot t}{(10^{-4}pc)^2 \cdot c \cdot t} \sim \frac{10^{46}}{10^{39}} = 10^7 \text{erg/cm}^3. \tag{6.15}$$

Our calculation so far only consider the toy model ignoring the jet divergence. But in fact the jet divergence happens and the magnetic field and plasma density descend as $1/r^2$. As a result the ω_c/ω_p ratio decreases as a function of $1/r$ since $\omega_c \propto B_0 \propto 1/r^2$ and $\omega_p \propto \sqrt{n} \propto 1/r$. When the magnetowaves with phase velocity $v_{ph} \sim c$ propagate into a low ω_c/ω_p (v_{phi}) region, the mode conversion process will take place[82] and the magnetowaves will be converted into the normal electromagnetic waves to keep traveling.

Based on that argument, it is possible to estimate the luminosity of magnetowave from the observed radio wave luminosity of AGN, since the frequency of magnetowave is in the range of radio wave if we take the magnetowave frequency $\omega \sim \omega_c/2$ for convenience. According to [83, 84], the observed differential luminosity to classify the low and high luminosity classes is

$$\frac{\partial^2}{\partial\nu\partial\Omega}L_{178MHz} = 10^{25}WHz^{-1}sr^{-1}, \tag{6.16}$$

at frequency 178 MHz. We are safe to take the frequency as the lower bound of magnetowave frequency. Therefore the total magnetowave luminosity is given by

$$L_{mag} = 10^{25} \times 10^7 \times \frac{\omega_c}{2 \cdot 2\pi}\text{erg} \cdot \text{s} \sim 10^{42}\text{erg} \cdot \text{s} \tag{6.17}$$

and we can deduce the energy fraction η of the order of $(10^{-3} - 10^{-4})$ from the ratio of the magnetowave luminosity to the total AGN luminosity $\sim 10^{46}\text{erg} \cdot \text{s}$. The a_0 in turn can be calculated from Eq. (6.14)

$$
\begin{aligned}
a_0 &= \sqrt{4\pi\eta\left(\frac{\epsilon_{AGN}^2}{4\pi}\right)\left(\frac{e}{m_e c\omega}\right)^2} \\
&= \sqrt{10^{-3} \sim 10^{-4}} \sim 0.1.
\end{aligned} \tag{6.18}
$$

Since $a_0 \sim 0.1 \ll \omega_c/\omega - 1 = 1$, the MPWA process is in the linear regime and the accelerating gradient G can be calculated from Eq.(4.10)

$$G = \frac{a_0^2}{(1 - \frac{\omega_c}{\omega})^2}\chi e E_{wb} \sim \text{O}(10^2)(\text{eV/cm}) \tag{6.19}$$

with the form factor χ of order 1 and $E_{wb} \sim 10^5$ V/cm for $n_0 \sim 10^{10}$cm^{-3} . We notice that the accelerating gradient G is obtained with the parameters taken in the jet rest frame.

For protons to reach energy $\epsilon = 10^{21}$ eV in our frame, it only requires energy gain 10^{20} eV in the jet frame with Γ of bulk motion typically being 10. Thus under the most optimized condition, the minimum distance for the protons to accomplish $\epsilon = 10^{20}$ eV is 10^{18} cm ($\simeq 0.3$ pc) in the jet frame, corresponding to $\epsilon = 10^{21}$ eV for 3 pc in our frame. It is quite tiny compared to the typical AGN jet length.

Chapter 7

Conclusions

We have established a novel acceleration mechanism for UHECR which is based on the wakefield excited by magnetowaves in astrophysical jets. The magnetowave itself is a medium wave and has a lower phase velocity than the speed of light. To have a good accelerating performance, we focus on the high frequency and high phase velocity whistler wave. It was shown that a high ω_c/ω_p ratio is the condition for MPWA, with which the dispersion relation of the whistler pulse tends to be linear with a slope close to the speed of light. We have formulated the nonlinear magnetowave induced plasma wakefield and confirmed it via the computer simulation. On the application to UHECR production, the magnetowaves are generated randomly. We expect a power spectrum for UHECR resulting from the stochastic particle wakefield interactions. Regarding AGN as the working source, we have estimated the accelerating gradient by putting physical parameters of AGN and finally concluded an optimized acceleration length required for particles to ZeV.

To summarize the content of the thesis, in chapter 2, we have introduced the basic concept of plasma from its definition, dynamics and the dielectric properties for waves. Plasma is a partially ionized gas. Having the quasi-neutrality and collective behaviors, the plasma can be defined following the three criteria, $\lambda \ll L$, $g \ggg 1$ and $\omega\tau > 1$. Plasma can be described by using fluid and kinetic approaches which are equivalent for solving problems. Since most problems in plasma can be solved regarding plasma as a fluid, we have used

the complete set of fluid equations to study the physics of plasma, particularly electrostatic wave and electromagnetic wave in plasma. In the last part, we introduced the plasma wakefield acceleration and the three types of driving pulses for wakefield excitation.

In chapter 3 and 4, we have studied the plasma wakefield acceleration in magnetized plasma in high and low frequency branches. In chapter 3, we discuss the case with $\omega/\omega_c \gg c$ in which the dispersion relation approaches the unmagnetized case and the magnetized effect can be ignored. We compared the results of plasma wakefield with $a_0 \ll 1$ (linear) and $a_0 \geq 1$ (nonlinear) respectively. In the linear regime, the plasma wake goes like a sinusoidal wave with the maximum amplitude linearly proportional to a_0^2. Whereas, in the nonlinear regime, the plasma within the pulse is totally expelled from the laser center and piled up to form a peak that leads to a sawtooth-like wakefield with amplitude proportional a_0. Taking the driving pulse as a square circularly polarized pulse, we analytically derived the plasma wakefield from the second order differential equation. The maximum of plasma wakefield amplitude was $a_0/\sqrt{1 + a_0^2}$, so the accelerating gradient $G \propto a_0^2$ while $a_0 \ll 1$ and $G \propto a_0$ while $a_0 \gg 1$.

In chapter 4, we studied the case for pulse frequency $\omega < \omega_c$ (MPWA theory). To implement the acceleration mechanism in this range, the MPWA condition $\omega_c/\omega_p \gg 1$ was made. We concentrated on the whistler modes and calculated the plasma wakefield in linear and nonlinear regime. With introducing the ponderomotive force, we have derived the linear plasma wakefield, whose amplitude contains an additional factor $(1 - \omega_c/\omega)$ to the ordinary G obtained without an external magnetic field. In the nonlinear regime, we made the MPWA condition contain γ factors. The plasma wakefield was solved from a full complete set of relativistic fluid equations and was also shown a sawtooth-like behavior. When the strength of background magnetic field B_0 increases, G decreases because $\omega_c/\omega > 1$, opposed to the laser case. Since there exists a singularity at $1 + \phi \to \omega_c/\omega_p$, we would make an upper limit on a_0. Beyond that the plasma becomes unstable. Then considering the upper limit on a_0, we have predicted the maximum accelerating gradient that MPWA can reach.

In chapter 5, we performed the particle-in-cell simulation to verify this MPWA theory. A code named "em1da" written by R. Sydora was used. In

our simulation, we compared two cases with different ω_c/ω_p ratios, 6 and 12. With successfully self-generated whistler wavepackets, we have confirmed the excitation of plasma wakefield and the validity of our MPWA theory. We have also showed that the whistler wavepacket sustains a longer distance with a higher ω_c/ω_p, i.e., it is less vulnerable to the dispersion. This aspect is especially important for MPWA to be a viable mechanism for terrestrial accelerator since it is essential for an accelerated particle to continuously gain energy from the plasma wakefield in order to attain a high energy[85].

Finally with the MPWA theory established, we apply the mechanism to UHECR. In chapter 6, we have shown that the power law spectrum can be deduced from the stochastic interactions between the test particle and the accelerating-decelerating phases of the wakefield. Without taking the dissipating process into account, the power law index is ideally given as -2. Next we discussed the possible sources for UHECR generation and the most recent observations from Pierre Auger and HiRes. So far this issue is still not settled. We invoked the AGN as a possible source and modeled the jet as a cylinder. From the parameters estimated near the AGN core and the observed luminosity of radio waves, we have obtained the accelerating gradient of MPWA in AGN jet. It enables a particle to possibly gain energy above 10^{21} eV in a short distance compared to the total jet length.

In this thesis we have shown the validity of MPWA for UHECR production with a power law spectrum and a linear accelerating gradient. But as a fist step we only simulated the process with a Gaussian magnetowave profile. However it is desirable to investigate our mechanism with magneto-shocks instead, which is astrophysically more relevant. Then the investigation of the generation of magnetoshocks in the plasma outflows becomes crucial to the next step. In addition, due to the involvement of the background magnetic field, MPWA should be taken as a fundamental phenomena in plasma physics. We have derived the plasma wakefield with the full relativistic fluid equations, but the other nonlinear phenomena of plasma magnetowave interaction should be investigated in detail. It would be extremely exciting if proof-of-principle experiments on MPWA can be pursued. With regard to the possible physical mechanism to excite the whistler magnetowave driving pulse for experimentation, it has been

shown that a fast ion-acoustic wave can decay into a whistler wave plus an ion-acoustic wave[86]. It is therefore conceivable that such a decay process, or conversely the fusion of two ion-acoustic waves, can produce whistler wave. Inspired by this, one wonders if a similar process can occur between a light wave and a whistler wave. If so, then perhaps a laser pulses could be converted into a whistler wave pulse in a magnetized plasma under suitable conditions.

Bibliography

[1] J. Linsley et al. *Phys. Rev. Lett.*, 10:146, 1963.

[2] J. Bird et al. *Phys. Rev. Lett.*, 71:3401, 1993.

[3] M. Tadeda et al. *Phys. Rev. Lett.*, 81:1163, 1998.

[4] K. Greisen. *Phys. Rev. Lett.*, 16:748, 1966.

[5] G. T. Zatsepin and V. A. Kuzmin. *JETP Lett.*, 4:78, 1966.

[6] J. Belz et al. (FLASH Collaboration). *Astropart. Phys.*, 25:57, 2006.

[7] M. Ave et al. (AIRFLY Collaboration). *Astropart. Phys.*, astro-ph/ 0703132.

[8] R. U. Abbasi et al. (HiRes Collaboration). *Phys. Rev. Lett.*, 100:101101, 2008.

[9] J. Abraham et al. (Pierre Auger Collaboration). *Phys. Rev. Lett.*, 101:061101, 2008.

[10] A. V. Olinto. *Phys. Rep.*, 329:333, 2000.

[11] A. V. Olinto et al. White Paper on Ultra-High Energy Cosmic Rays. 2009. arXiv:astro-ph/0903.0205.

[12] Dmitry V. Semikoz and Gunter Sigl. *JCAP*, 0404:003, 2004, hep-ph/0309328.

[13] E. Fermi. *Phys. Rev.*, 75:1169, 1949.

[14] A. R. Bell. *Mon. Not. R. Astron. Soc.*, 182:147–156, 1978.

[15] R. D. Blandford and J. P. Ostriker. *Astrophys. J.*, 221:L29, 1978.

[16] G. Skadron W. I. Axford, E. Leer. In *15th International Cosmic Ray Conference, at Plovdiv, Bulgaria, August 13-26, 1977*, volume 11, page 132.

[17] G. F. .Krymskii. *Sov. Phys. G*, 22:327, 1977.

[18] Thomas K. Gaisser. *Cosmic Rays and Particle Physics.* Combridge University Press, New York, 1990.

[19] Y. A. Gallant. astro-ph/0201243.

[20] M. Vietri. *Astrophys. J.*, 453:883, 1995.

[21] Y. A. Gallant J. G. Kirk, A. W. Guthmann and A. Achterberg. *Astrophys. J.*, 542:235, 2000.

[22] Matthew G. Baring. *Nuclear Physics B (Proc. Suppl.)*, 136:198, 2004.

[23] K. Koyama et al. *Nature*, 378:255, 1995.

[24] J. M. Dawson T. Tajima. *Phys. Rev. Lett.*, 43:267, 1979.

[25] Pisin Chen et al. *Phys. Rev. Lett.*, 54:693, 1985.

[26] T. Tajima P. Chen and Y. Takahashi. *Phys. Rev. Lett.*, 89:161101, 2002.

[27] Masahiro Hoshino. *Astrophys. J.*, 672:940–956, 2008.

[28] P. K. Shukla M. E. Dieckmann and B. Eliasson. *Phys. Plasmas*, 13:062905, 2006.

[29] Guey-Lin Lin Rober Noble Feng-Yin Chang, Pisin Chen and Richard Sydora. *Phys. Rev. Lett.*, 102:111101, 2009.

[30] Francis F. Chen. *Introduction to Plasma Physics.* Plenum Press, New York, 1st, edition, 1974.

[31] Lewi Tonks and Irving Langmuir. *Phys. Rev.*, 33:195, 1929.

[32] E. Esarey et al. *IEEE Trans. Plasma Sci.*, 24:252, 1996.

[33] J. T. MendonMand P. K. Shukla R. Bingham. *Plasma Phys. Control. Fusion*, 46:R1–R23, 2004.

[34] Donald Umstadter. *Plasma Phys.*, 8:1774, 2001.

[35] R.Noble. *Phys. Rev. A*, 32:460, 1985.

[36] K. Nakajima et al. *Phys. Rev. Lett.*, 74:7728, 1995.

[37] C. Coverdale et al. *Phys. Rev. Lett.*, 74:7659, 1995.

[38] A. Modena. *Nature*, 337:606, 1995.

[39] V. I. Kirsanov A. A. Pogosova N. E. Andreev, L. M. Gorbunov and R. R. Ramazashvili. *Pisma Zh. Eksp. Teor. Fit*, 55:551–555, 1992.

[40] Jr. T. M. Antonsen and P. Mora. *Phys. Rev. Lett.*, 69:2204–2207, 1993.

[41] E. Esarey P. Sprangle J. Krall, A. Ting and G. Joyce. *Phys. Rev. E*, 48:2157–2161, 1993.

[42] Ronald D. Ruth and Pisin Chen. *SLAC-PUB*, page 3910, 1986.

[43] P. K. Shukla. *Physica Scripta*, T52:73, 1994.

[44] Pisin Chen. *Part.Accel.*, 20:171–182, 1987.

[45] E. Esarey P. Sprangle and A. Ting. *Phys. Rev. A*, 41:4463, 1990.

[46] Eric Esarey and Carl B. Schroeder. *LBNL Report, LBNL=53510*, 2003.

[47] J. Aron C. Max and A. B. Langdon. *Phys. Rev. Lett.*, 33:209, 1974.

[48] K. H. Spetchek. *J. Plasma Phys*, 18:298, 1977.

[49] Y. C. Lee G. Z. Sun, E. Ott and P. Guzdar. *Phys. Fluid*, 3:526, 1987.

[50] W. B. Mori T. Katsouleas S. C. Wilks, J. M. Dawson and M. E. Jones. *Phys. Rev. Lett.*, 62:2600, 1989.

[51] A. Ting E. Esarey, E. Esarey P. Sprangle, and A. Ting. *NRL Memo Report*, 1989. 6541.

[52] T. Tajima J. M. Dawson M. Ashour-Abdalla, J. N. LeBoeuf and C. F. Kennel. *Phys. Rev. A*, 23:1906, 1981.

[53] C. J. McKinstrie and E. A. Startsev. *Phys. Rev. E*, 54:R1070, 1996.

[54] V. I. Kirsanov S. V. Bulanov and A. S. Sakhanov. *Pis'ma Zh. Eksp. Teor. Fiz*, 4:176, 1989.

[55] V.I. Berezhiani and I.G. Murusidze. *Phys. Lett. A*, 148:338, 1990.

[56] V.I. Berezhiani and I.G. Murusidze. *Physica Scripta*, 45:87, 1992.

[57] H.Washimi and V. I. Karpman. *Zh. Eksp. Teor. Fiz.*, 71:1010, 1976.

[58] G. Statham and D. ter Haar. *Plasma Phys.*, 25:681, 1983.

[59] L. M. Gorbnnov and V. I. IOrsanov. *Zh. Eksp. Teor. Fiz.*, 93:509, 1987.

[60] F. Y. Chang et al. in preparsion.

[61] O. Buneman. *Phys. Rev.*, 115:503, 1959.

[62] J. M. Dawson. *Phys. Fluids*, 5:445, 1962.

[63] J. P. Verboncoeur. *Plasma Phys. Control. Fusion*, 47:A231, 2005.

[64] A. B. Landan and C. K. Birdsall. *Plasma Physics via Computer Simulation*. Taylor Francis, New York.

[65] R. W. Hockney and J. W. Eastwood. *Computer Simulation Using Particles*. McGraw-Hill, New York, 1981.

[66] J. M. Dawson. *Rev. Mod. Phys.*, 55:403, 1983.

[67] R. D. Sydora. *J. Comp. Appl. Math.*, 109:243, 1999.

[68] T. Tajima. *Computational Plasma Physics with Applications to Fusion and Astrophysics*. Addison-Wesley.

[69] J. P. Boris. Relativistic plasma simulation-optimization of a hybrid code. Proceedings of the Fourth Conference on Numerical Simulation of Plasmas, Naval Res. Lab., Washington, DC, 1970.

[70] T. Tajima K. Mima, W. Horton and A. Hasegawa. Proceedings of Nonlinear Dynamics and Particle Acceleration., AIP, 1991.

[71] Toshiki Tajima Pisin Chen and Yoshiyuki Takahashi. astro-ph/0205287.

[72] D. De Marco and T. Stanev. *Phys. Rev. D*, 72:081301, 2005, astro-ph/0506318.

[73] A. M. Hillas. *Ann. Reo. Astron. Astrophys.*, 22:425, 1984.

[74] Eli Waxman. *Phys. Rev. Lett.*, 75:386, 1995.

[75] M. Vietri. *Astrophys. J.*, 453:883, 1995.

[76] J. Rachen and P. Biermann. *Astron. Ap*, 272:161, 1993.

[77] A. Z. Gazizov V. S. Berezinsky and S. I. Grigorieva. *Phys.Lett. B*, 612:147, 2005.

[78] J. Abraham et al. (Pierre Auger Collaboration). *Science*, 318:939, 2007. arXiv:astro-ph/0711.2256.

[79] J. Abraham et al. (Pierre Auger Collaboration). arXiv:astro-ph/0712.2843.

[80] R. U. Abbasi et al. (HiRes Collaboration). arXiv:astro-ph/0804.0382v2.

[81] M. C. Begelman M. J. Rees and R. D. Blandford. *Annals of the New York Academy of Sciences*, 375:254, 1981.

[82] Thomas H. Stix. *Phys. Rev. Lett.*, 15:878, 1965.

[83] E. Ros T. Arshakian and A. Zensus. astro-ph/0608172.

[84] T. J. Pearson J. V. Wall and M. S. Longair. *Mon. Not. R. Astron. Soc.*, 193:683, 1980.

[85] G. L. Lin R. J. Noble P. Chen, F.Y. Chang and R. Sydora. *Plasma Phys. Control. Fusion*, 51:024012, 2009. arXiv:physics.acc-ph/0808.3036.

[86] R. Bharuthram and M. Y. Yu. *Astrophys. Space Sci.*, 146:355, 1988.

Appendix A

Transverse Fluid

Momentum Equation

When an electromagnetic wave in magnetized plasma propagates parallel to the external magnetic field B_0 along z direction, the plasma motions associated with the EM fields can be described as,

$$\frac{d\gamma\beta_x}{dt} = -\frac{e}{mc}E_x - \beta_y\omega_c + \frac{e}{m}\frac{\beta_z}{c}B_y \qquad (A.1)$$

$$\frac{d\gamma\beta_y}{dt} = -\frac{e}{mc}E_y + \beta_x\omega_c - \frac{e}{m}\frac{\beta_z}{c}B_x, \qquad (A.2)$$

where $\gamma = (1 - \beta_x^2 - \beta_y^2 - \beta_z^2)^{-1}$ is the Lorentz factor of the plasma motions and $\omega_c \equiv eB_0/mc$ is the electron cyclotron frequency. It is convenient to further express the above equations in terms of the normalized vector potential **a** that is related to $\mathbf{E}_\perp$ and $\mathbf{B}_\perp$ from Maxwell equations,

$$\frac{d\gamma\beta_x}{dt} = \frac{\partial a_x}{\partial t} + c\beta_z\frac{\partial a_x}{\partial z} - \beta_y\omega_c = \frac{da_x}{dt} - \beta_y\omega_c \qquad (A.3a)$$

$$\frac{d\gamma\beta_y}{dt} = \frac{\partial a_y}{\partial t} + c\beta_z\frac{\partial a_y}{\partial z} + \beta_x\omega_c = \frac{da_y}{dt} + \beta_x\omega_c, \qquad (A.3b)$$

where the total time derivative $d/dt = \partial/\partial t + c\beta_z\partial/\partial z$. Since the electromagnetic wave becomes circularly polarized when travels along the magnetic field, we assume a right-handed polarized wave that have $\beta_\perp = \beta_x + i\beta_y$ and $a = a_x + ia_y$. Then we multiply Eq. (A.3b) by i and add the result to Eq. (A.3a), we obtain the simplified form of the equation of motion for $\beta_\perp$

$$\frac{d}{dt}(\gamma\beta_\perp - a) = -i\omega_c\beta_\perp. \qquad (A.4)$$

To solve the equation, we decompose the plasma responses to the driving pulse into slow and fast parts and assume that $\beta_\perp = \beta_{\perp s} \exp[ik\zeta]$ to respond to the electric field $E_{\perp s} \exp[ik\zeta]$. $E_{\perp s}$ is the envelop of the driving pulse and $\exp[ik\zeta]$ is the fast oscillation part. Assuming that β_z varies according to the scale of the pulse envelop, $\beta_z = \beta_{zs}$, we arrive at

$$\frac{\partial}{\partial \zeta}(\gamma \beta_\perp - a) = i \frac{\omega_c}{c} \frac{\beta_{\perp s}}{1 - \beta_{zs}} e^{ik\zeta}$$

by inserting $\beta_\perp$ into Eq. (A.4). Sequently $\beta_\perp$ is solved from integration by part and it reads,

$$\gamma \beta_\perp - a = \frac{\omega_c}{kc} \frac{\beta_\perp}{1 - \beta_z} + i \frac{\omega_c}{k^2 c} \frac{\partial}{\partial \zeta} \left(\frac{\beta_{\perp s}}{1 - \beta_{zs}} \right) e^{ik\zeta} + \cdots$$

where the second term on the right hand is expected to be suppressed compared to the first term (quasistatic approximation). Finally we obtain the relation between $\beta_\perp$ and a,

$$\beta_\perp = \frac{a}{\left| \gamma - \frac{\omega_c}{\omega(1 - \beta_z)} \right|}. \tag{A.5}$$

Having this relation substituted into into the wave equation of a in Eq. (3.3), we arrive at

$$\left[\frac{\partial^2}{\partial z^2} - \frac{1}{c^2} \frac{\partial^2}{\partial t^2} \right] \mathbf{a} = k_p^2 \boldsymbol{\beta}_\perp = k_p^2 \frac{\mathbf{a}}{\gamma - \frac{\omega_c}{\omega}}$$

$$\left[-k^2 + \frac{\omega^2}{c^2} - \frac{\omega_p^2}{c^2} \frac{1}{\gamma - \frac{\omega_c}{\omega}} \right] \mathbf{a} = 0.$$

by putting $n = n_0$ and $a \propto \exp[i(kz - \omega t)]$ for a plane wave. Therefore the relativistic dispersion relation of magnetowave is obtained,

$$\omega^2 = c^2 k^2 + \frac{\omega_p^2 / \gamma}{1 - \omega_c / \gamma \omega}. \tag{A.6}$$

Appendix B

Differential Equation of Nonlinear MPWA

The integration of the complete fluid equations for MPWA in (ζ, τ) coordinate system leads to

$$\phi - \gamma(1 - \beta_z) = -1, \qquad \text{(B.1a)}$$

$$n(1 - \beta_z) = n_0, \qquad \text{(B.1b)}$$

which is similar to the form in unmagnetized case. Therefore the relation between n, n_0, γ and ϕ is given

$$\frac{n}{n_0} = \frac{\gamma}{1 + \phi} = \frac{1}{1 - \beta_z}. \qquad \text{(B.2)}$$

We have the Poisson equation (Eq. (4.15a)) rewritten as

$$
\begin{aligned}
\frac{\partial^2 \phi}{\partial \zeta^2} &= k_p^2 (\frac{n}{n_0} - 1) \\
&= k_p^2 (\frac{1}{1 - \beta_z} - 1) \\
&= k_p^2 (\frac{\beta_z}{1 - \beta_z}). \qquad \text{(B.3)}
\end{aligned}
$$

The main difference between with and without magnetic field cases is on the γ factor. With $\beta_\perp$ solved in terms of a (Eq. (4.19))

$$\beta_\perp = \frac{a}{|\gamma - \frac{\omega_c}{\omega(1 - \beta_z)}|}, \qquad \text{(B.4)}$$

we have

$$\gamma^2 \beta_\perp^2 = \gamma^2(1 - \beta_z^2) - 1 = \frac{a^2}{\left(1 - \frac{\omega_c}{\omega\gamma(1 - \beta_z)}\right)^2}$$

and

$$\gamma^2(1 - \beta_z^2) = \frac{a^2}{\left(1 - \frac{\omega_c}{\omega(1 + \phi)}\right)^2} + 1 \tag{B.5}$$

Squaring Eq. (B.1a), we get

$$\gamma^2(1 - \beta_z)^2 = (1 + \phi)^2. \tag{B.6}$$

So that the combination of Eq. (B.5) and (B.6) results in

$$\left(\frac{a^2}{1 - \frac{\omega_c/\gamma\omega}{1 - \beta_z}} + 1\right)\left(\frac{(1 - \beta_z)^2}{1 - \beta_z^2}\right) = (1 + \phi)^2$$

which can be rearranged as

$$\frac{1 + \beta_z}{1 - \beta_z} = 1 + 2\frac{\beta_z}{1 - \beta_z} = \left(\frac{a^2}{1 - \frac{\omega_c/\omega}{1 + \phi}} + 1\right)\frac{1}{(1 + \phi)^2}. \tag{B.7}$$

The Poisson equation is finally obtained,

$$\frac{\partial^2 \phi}{\partial \zeta^2} = \frac{k_p^2}{2}\left[\left(\frac{a^2}{(1 - \frac{\omega_c}{\omega(1 + \phi)})^2} + 1\right)\frac{1}{(1 + \phi)^2} - 1\right]. \tag{B.8}$$

87